MCB
Journals.ASM.org

The Stationary-Phase Cells of *Saccharomyces cerevisiae* Display Dynamic Actin Filaments Required for Processes Extending Chronological Life Span

Pavla Vasicova, Renata Lejskova, Ivana Malcova, Jiri Hasek

Laboratory of Cell Reproduction, Institute of Microbiology of ASCR, Prague, Czech Republic

Stationary-growth-phase *Saccharomyces cerevisiae* yeast cultures consist of nondividing cells that undergo chronological aging. For their successful survival, the turnover of proteins and organelles, ensured by autophagy and the activation of mitochondria, is performed. Some of these processes are engaged in by the actin cytoskeleton. In *S. cerevisiae* stationary-phase cells, F actin has been shown to form static aggregates named actin bodies, subsequently cited to be markers of quiescence. Our *in vivo* analyses revealed that stationary-phase cultures contain cells with dynamic actin filaments, besides the cells with static actin bodies. The cells with dynamic actin displayed active endocytosis and autophagy and well-developed mitochondrial networks. Even more, stationary-phase cell cultures grown under calorie restriction predominantly contained cells with actin cables, confirming that the presence of actin cables is linked to successful adaptation to stationary phase. Cells with actin bodies were inactive in endocytosis and autophagy and displayed aberrations in mitochondrial networks. Notably, cells of the respiratory activity-deficient *cox4*Δ strain displayed the same mitochondrial aberrations and actin bodies only. Additionally, our results indicate that mitochondrial dysfunction precedes the formation of actin bodies and the appearance of actin bodies corresponds to decreased cell fitness. We conclude that the F-actin status reflects the extent of damage that arises from exponential growth.

Once glucose and other external nutrients are exhausted, cell division stops and *Saccharomyces cerevisiae* cells are able to survive for extended periods of time. This period of survival has been termed chronological aging and has become a model for aging of postmitotic tissues (1, 2). The cells in these nondividing stationary-phase cell cultures are often termed quiescent (Q) cells (3, 4). Some authors claim that stationary-phase yeast cell populations are heterogeneous and only a portion of them have characteristics of quiescence (5, 6). The ability to survive the period of scarcity of external nutrition and reproduce again upon refeeding is influenced by several life span-extending genetic and environmental interventions. One of the most cited is calorie restriction (CR) (7).

In general, cells that are in a nutrient-poor environment activate processes that help them to efficiently utilize inner resources and thus prolong the life span. A catabolic process that has a positive impact on chronological aging is autophagy, which provides nutrients by the vacuolar degradation of damaged or superfluous macromolecules and organelles (8, 9). In addition, Fabrizio et al. demonstrated that the deletion of several genes encoding endosomal functions also shortens the life span (8). Note that some of them have not been directly implicated in autophagy (8). The efficient utilization of resources is ensured by the activation of mitochondrial respiration. It has been proved that the utilization of carbohydrate stores by respiration instead of glycolysis extends the life span (10, 11), and mitochondrial dysfunctions cause its shortening (12). Endosome movement, selective types of autophagy, and the quality control of mitochondria are engaged in by the actin cytoskeleton (13–15).

The actin cytoskeleton has been studied in various types of eukaryotic cells. It is generally accepted to play a key role in essential cellular processes, including movement, protein trafficking and secretion, cell division, and growth. In the yeast *S. cerevisiae*, the actin cytoskeleton is composed of three morphologically distinct structures: cortical actin patches (here referred to as patches), actin cables (here referred to as cables), and the actomyosin ring (16). Patches, sites of endocytic plasma membrane uptake, are networks of branched actin filaments (17). The actin turnover in these structures provides the force required for nonlinear cortical patch movement and for elongation of membrane invagination (18, 19). The rapid linear movement of patches, which is typical for the last step of endocytosis, is mediated by cables (13, 18). The cables are long bundles of short overlapping actin filaments that serve as tracks for a molecular motor-dependent transport of various cargoes (20). Their assembly depends on formins Bni1 and Bnr1 (21), whose localization is cell cycle dependent (22).

The yeast actin cytoskeleton is responsive to environmental stresses. Therefore, it is regarded as a sensor, as changes of its status are linked to the cell's fate (23). The actin cytoskeleton is transiently depolarized upon heat shock (24, 25) and osmotic stress (26, 27). The formation of oxidized actin bodies during acute oxidative stress has been reported (28). The F-actin aggregates, named actin bodies, were observed in stationary-phase cells, and their occurrence has been linked to quiescence (4). On the

Received 19 August 2015 **Accepted** 31 August 2015

Accepted manuscript posted online 8 September 2015

Citation Vasicova P, Lejskova R, Malcova I, Hasek J. 2015. The stationary-phase cells of *Saccharomyces cerevisiae* display dynamic actin filaments required for processes extending chronological life span. Mol Cell Biol 35:3892–3908. doi:10.1128/MCB.00811-15.

Address correspondence to Pavla Vasicova, pavla.vasicova@img.cas.cz, or Jiri Hasek, hasek@biomed.cas.cz.

Supplemental material for this article may be found at http://dx.doi.org/10.1128/MCB.00811-15.

TABLE 1 Yeast strains constructed in this study

Strain	Genotype[a]
CRY1673	*MAT***a** *his3Δ1 leu2Δ0 met15Δ0 ura3Δ0 ABP140-GFP::HIS3MX6*
CRY1778	*MAT***a** *his3Δ1 leu2Δ0 met15Δ0 ura3Δ0 cox4::URAMX*
CRY1872	*MAT***a** *his3Δ1 leu2Δ0 met15Δ0 ura3Δ0 ABP1-EGFP::HIS3MX6 SAC6-mCherry::natNT2*
CRY1886	*MAT***a** *his3Δ1 leu2Δ0 met15Δ0 ura3Δ0 ABP140-EGFP::HIS3MX6 SAC6-mCherry::natNT2*
CRY1959	*MAT***a** *his3Δ0 leu2Δ0 met15Δ0 ura3Δ0 WHI5-GFP::HIS3MX6 ABP140-TagRFP-T::natNT2*
CRY1978	*MAT***a** *his3Δ1 leu2Δ0 met15Δ0 ura3Δ0 cox4::URAMX ABP140-EGFP::HIS3MX6*
CRY2097	*MAT***a** *his3Δ0 leu2Δ0 met15Δ0 ura3Δ0 TOM20-GFP::HIS3MX6 ABP140-TagRFP-T::natNT2*
CRY2098	*MAT***a** *his3Δ0 leu2Δ0 met15Δ0 ura3Δ0 RSM23GFP::HIS3MX6 ABP140-TagRFP-T::natNT2*
CRY2115	*MAT***a** *his3Δ0 leu2Δ0 met15Δ0 ura3Δ0 MYO2-GFP::HIS3MX6 ABP140-TagRFP-T::natNT2*
CRY2116	*MAT***a** *his3Δ0 leu2Δ0 met15Δ0 ura3Δ0 TOM20-GFP::HIS3MX6 ABP140-TagRFP-T::natNT2 cox4::URAMX*
CRY2134	*MAT***a** *his3Δ1 leu2Δ0 met15Δ0 ura3Δ0 ABP140-TagRFP-T::natNT2*/pRS316 *GFP-ATG8*

[a] EGFP, enhanced green fluorescent protein.

other hand, the formation of actin aggregates after the reduction of actin dynamics in post-diauxic-phase cells leads to the dysfunction of mitochondria followed by apoptosis (29). Notably, most of these observations were obtained on fixed cells using phalloidin staining of F actin.

Live-imaging analyses of cables labeled by actin binding protein Abp140 fused to green fluorescent protein (GFP) significantly extended common knowledge about the dynamics and persistence of cables. The work of Yu et al. revealed the different dynamics and motility of cables in polarized and unpolarized cells in the exponential phase (30). Additionally, *in vivo* observations of cables under conditions of acute glucose depletion revealed the stabilization of cables (31), albeit previous observations of fixed cells detected the persistence of depolarized patches only (32). This *in vivo* approach has not yet been used for monitoring of actin cables in post-diauxic and stationary phases.

Here we report, with the help of only *in vivo* observations of the actin cytoskeleton, that stationary-phase cultures consist of two live cell subpopulations, namely, cells with a dynamic actin cytoskeleton and cells with static actin bodies. This heterogeneity was observed under various conditions of cultivation (in synthetic complete medium, in rich yeast extract, peptone, and glucose [YPD] medium, and under conditions of calorie restriction). The cells with dynamic actin displayed active endocytosis and autophagy and a well-developed mitochondrial network. On the contrary, in cells with actin bodies, endocytosis and autophagy were inactive and these cells contained an aberrant mitochondrial network. Similar changes to the shape of the mitochondria were visible in respiratory activity-deficient cells of a *cox4*Δ strain. The majority of these respiratory activity-deficient cells contained actin bodies in early stationary phase. As the presence of actin cables is linked to a well-developed mitochondrial network, we conclude that the occurrence of a dynamic actin cytoskeleton indicates successful adaptation for survival in stationary phase.

MATERIALS AND METHODS

Yeast strains, plasmids, and growth conditions. Unless specified otherwise, yeast cells were grown in synthetic complete (SC) medium (0.17% yeast nitrogen base without amino acids and ammonium sulfate, 0.5% ammonium sulfate, and a complete or appropriate mixture of amino acids supplemented with 2% or 0.5% glucose) at 25°C for up to 7 days or 12 days. For the observation of cables in post-diauxic phase/stationary phase in rich medium, yeast cultures were grown in YPD medium (1% yeast extract, 2% peptone, 2% glucose) at 30°C. The starting concentration of cells for long-term cultivations was 5×10^6 cells/ml. Cells were cultivated in 10 ml of SC medium in 100-ml Erlenmeyer flasks. For selection, the respective amino acid was omitted from the dropout mix or the appropriate antibiotic was added to the medium. Survival plating was done on YPD agar plates (2% agar) incubated for 3 to 5 days at 28°C, depending on the strain. For recovery of the actin cytoskeleton, fresh SC medium was added directly to pelleted aged cells that had already been positioned on a glass slide. Standard methods were used for all DNA manipulations.

The newly constructed stains used in this study are listed in Table 1. All strains used in this study are isogenic to strain BY4741 (*MAT***a** *his3Δ1 leu2Δ0 met15Δ0 ura3Δ0*), available from Euroscarf. Yeast strains carrying GFP fusions of the *BNI1*, *BNR1*, *MYO2*, *WHI5*, *TOM20*, and *RSM23* genes were obtained from Invitrogen (33). All other chromosomal tagging (GFP/mCherry/TagRFP-T) and deletions were created by one-step targeted integration of a DNA cassette created by PCR (34, 35). The correct integration was proved by PCR. Specifically, the *COX4* gene was deleted by use of a disruption cassette amplified from the vector pUG72 (36). The *ABP140* and *ABP1* genes were fused to GFP on its C terminus using a cassette that originated from the vector pKT128 (37). The genomic C-terminal mCherry fusion of the *SAC6* gene was created with a cassette that originated from the vector pFM699 (kindly provided by M. Farkasovsky, Slovak Academy of Sciences, Slovakia). The *ABP140* gene was also fused to the photostable TagRFP-T version of red fluorescent protein (RFP) (38) on its C terminus using a cassette that originated from the vector pIM700. The cassette was produced by inserting a SalI-BamHI fragment containing the gene encoding TagRFP-T, which was amplified by PCR, on pFA-TagRFP-T-URA3 (plasmid pEE10; a kind gift of M. Whiteway, McGill University, Montreal, Quebec, Canada) as the template into the vector pFM699. Details of the plasmid and strain constructions are available upon request. Centromeric plasmid pRS316 GFP-ATG8, used for the monitoring of autophagy, was kindly provided by Yoshinory Ohsumi (Tokyo Institute of Technology, Tokyo, Japan). Yeast transformation was done by high-efficiency yeast transformation (39). *Escherichia coli* strain DH5α [F^- *endA1 glnV44 thi-1 recA1 relA1 gyrA96 deoR nupG* ϕ80d*lacZ*ΔM15 Δ(*lacZYA-argF*)*U169*, *hsdR17*(r_K^- m_K^+) λ^-] was cultivated in LB medium (1% tryptone, 0.5% yeast extract, 1% NaCl) and used for plasmid propagation.

Growth curve, clonogenic assay, and cell viability. The strains were cultivated in SC medium at 25°C. The starting concentration of the cells was the same as that of the cells used for microscopic observations (5×10^6 cells/ml). To obtain the growth curve, the growth of the yeast culture was monitored by determining of the concentration of cells by the use of a CASY cell counter (Scharfe System) at the time points indicated below. Note that the volume of the stationary-phase cultures that had evaporated was refilled before every measurement of the concentration of the cells. The ability to reproduce was determined by a clonogenic assay. The concentration of cells was counted by the use of a CASY cell counter (Scharfe System), and after serial dilution, 150 cells were plated on YPD plates. Two

independent serial dilutions and three platings for every dilution were done. After 3 to 5 days, the CFU were counted and the percentage of reproducing cells was calculated. Alternatively, the amount of dead cells was measured via propidium iodide (PI; Sigma-Aldrich) staining. For PI staining, cells (0.5×10^7) were pelleted and resuspended in 100 μl of citrate buffer, and then PI (final concentration [f.c.], 30 μM) was added. Cells were incubated for 10 min in Eppendorf tubes in an Eppendorf mixer (25°C, 550 rpm) and then once washed with citrate buffer and imaged by wide-field microscopy at room temperature. The cells with an elevated PI fluorescence were counted, and their percentages were calculated.

Disruption of F actin using LatB treatment. (i) Sensitivity of the actin cytoskeleton to LatB in stationary-phase cells. Two- and 7-day-old cell cultures were diluted (2×10^7 cells/ml) using conditioned medium from a culture of the same age. Latrunculin B (LatB; Sigma-Aldrich) was added to a concentration of 20 μM, and the cells were incubated in an Eppendorf mixer (25°C, 550 rpm). Cells were imaged at the time points indicated below, and Abp140-GFP localization was determined.

(ii) Extent of GFP-Atg8 vacuolar accumulation after disruption of F actin. One-day-old cell cultures expressing GFP-Atg8 were diluted (2×10^7 cells/ml) with the conditioned medium, LatB was added to a final concentration of 100 μM, and these cells were incubated in 12-well plates in an Eppendorf mixer (25°C, 550 rpm) for an additional 1 day. The control cells were incubated with dimethyl sulfoxide (DMSO; 0.25%). The cells were imaged, and the intensity of GFP-Atg8 in the vacuole and in the cytoplasm was measured (for details, see "Autophagy" below).

Endocytosis. Endocytosis was monitored by determination of the internalization of the lipophilic dye FM4-64 (Invitrogen). Briefly, 200 μl of a 2- or 7-day-old cell culture was incubated with FM4-64 (f.c., 40 μM) for 100 min in an Eppendorf mixer (25°C, 550 rpm). Before imaging, the cells were washed with the conditioned medium. In experiments where the role of the actin cytoskeleton in FM4-64 internalization was tested, the cells were pretreated with LatB (f.c., 100 μM) for 30 min, and then FM4-64 was added and the cells were incubated for an additional 100 min.

Autophagy. The activation of autophagy was monitored by wide-field microscopy as GFP-Atg8 vacuolar accumulation. For quantification of the vacuolar/cytoplasmic (V/C) GFP-signal ratio, the GFP fluorescence and differential interference contrast (DIC) images were merged and then analyzed on an xcellence rt platform (Olympus Cell-R). Note that most of the cells in the stationary growth phase displayed a distinguishable vacuole on the DIC image. To obtain average gray values (mean fluorescence intensities) in the vacuole and in the cytoplasm, the same round region of interest (ROI) with a diameter 0.3 μm was used for both compartments. The values obtained were analyzed using GraphPad Prism (version 6) software.

Estimation of replicative age. Replicative age was determined by counting of the number of bud scars stained by calcofluor white M2R (CFW; Sigma-Aldrich). Two- and 7-day-old cell cultures (2×10^7 cells) were incubated with CFW (f.c., 25 μM) for 15 min. Then, the cells were washed with the conditioned medium and imaged. The cells were divided into 5 groups, daughter cells (cells with no scars) and mother cells (cells with 1 or 2, 3 or 4, 5 or 6, and 7 to 10 bud scars).

Fluorescence microscopy. The cells in the cultivation medium were inspected, mounted on a glass slide, covered with a coverslip, and directly imaged at room temperature. Only the first three snapshots of each sample were used for analysis. The distribution of various fusion proteins (fused to GFP, TagRFP-T, or mCherry) was analyzed with a 100× Planapochromat objective (numerical aperture [NA] = 1.4); the PI fluorescence for scoring of PI-positive cells was analyzed with an Olympus 60× Planapochromat objective (NA = 1.35). An Olympus IX-81 inverted microscope equipped with an Hamamatsu Orca/ER digital camera and an Olympus Cell R detection and analysis system was used. GFP fusions were detected using GFP filter block (U-MGFPHQ; maximum excitation, 488 nm; maximum emission, 507 nm); mCherry and TagRFP-T fusions, PI, and FM4-64 were detected using RFP filter block (U-MWIY2; maximum excitation, 545 to 580 nm; maximum emission, 610 nm); and was detected using blue fluorescent protein filter block (U-MFBFPHQ; maximum excitation, 390 nm; maximum emission, 460 nm). Images were processed and merged using Olympus Cell R (xcellence rt) and Adobe CS5 software. Images presented as z-stacks are maximal projections of stacks obtained using 0.6-μm steps. Images presented as T-stacks are the maximum-intensity projection of the fluorescence from all captured frames. Deconvolution of images obtained by z-sectioning was done by use of a Wiener filter (WF). Deconvolution of images obtained by time-lapse microscopy was done by use of a no-neighbor filter (NoNF).

Time-lapse setting. The image acquisition parameters were as follows: for the images in Fig. 4A, 5D, 10B, and 11, 1 frame/4.5 s for 130.5 s; for the images in Fig. 4B, 1 frame/1 s for 60 s; and for the images in Fig. 12C, 1 frame/4.5 s for 265.5 s.

Data reproducibility. In all graphs, bars indicate standard deviations. The number of independent experiments (*n*) from which the mean values were obtained is shown in each graph. In Fig. 1G and 12B, mean values of percent CFU were obtained from 6 plates (see the information on the clonogenic assay above). In Fig. 1B, 6B, 8C and D, and 9, representative graphs of three experimental repeats are shown. In Fig. 1D and G, 6B, 7B, and 12B, for each time point, more than 150 cells were scored for Abp140-GFP localization. In Fig. 9, for each time point, more than 400 cells were scored for the number of bud scars. In Fig. 1F and 7C, for each time point, more than 600 cells were scored for PI fluorescence. In Fig. 8C and D, the intensity of GFP-Atg8 fluorescence was measured in the vacuole and cytoplasm of more than 100 cells in each experiment.

RESULTS

The stationary growth phase of *S. cerevisiae* is associated with F-actin heterogeneity. The actin binding protein Abp140 fused to GFP has been successfully used to analyze the dynamics of cables in live exponentially growing *S. cerevisiae* cells, and these *in vivo* experiments noticeably extended existing knowledge about the yeast actin cytoskeleton (30, 40). We applied this *in vivo* labeling to inspect the reorganization of cables in chronologically aged cultures. First, we defined when the yeast cultures grown in synthetic complete (SC) medium at 25°C reach the stationary phase and revealed that such cell cultures reached the stationary phase on day 2, as the number of cells did not increase in the following days (Fig. 1A). The cessation of cell proliferation and achievement of the stationary growth phase were confirmed by nuclear localization of Whi5-GFP in the majority of 2-day-old cells (Fig. 1B). Note that Whi5 is the transcription repressor, and when it is localized in the nucleus, the G_1/S transition is repressed (41, 42). Then we analyzed the distribution of Abp140-GFP in the post-diauxic phase (1 day) and in the stationary phase (2 days and 7 days) (Fig. 1C and D). Compared to exponentially growing cultures containing only cells with cables, we found that 1-day-old cultures contained cell with cables (88% ± 3%), cells with actin accumulations named actin bodies (11% ± 2%) (4), and cells without the specific Abp140-GFP fluorescence (nonfluorescent [NF] cells; 1%). In cells with cables, the depolarized localization of Abp140-GFP into the patches was often seen. All three types of cells (cells with cables, cells with actin bodies, and NF cells) were present when the culture reached the stationary phase (2 days), but the proportion of each group changed. The amount of cells with cables was smaller (60% ± 6%) and the amount of cells with bodies and NF cells was larger (34% ± 7% and 5% ± 3%, respectively) in 2-day-old cultures than in 1-day-old cultures. Further chronological aging (7 days) caused additional changes in the proportions of all defined groups of cells. The amount of cells with cables and bodies decreased (48% ± 5% and 19% ± 9%, respec-

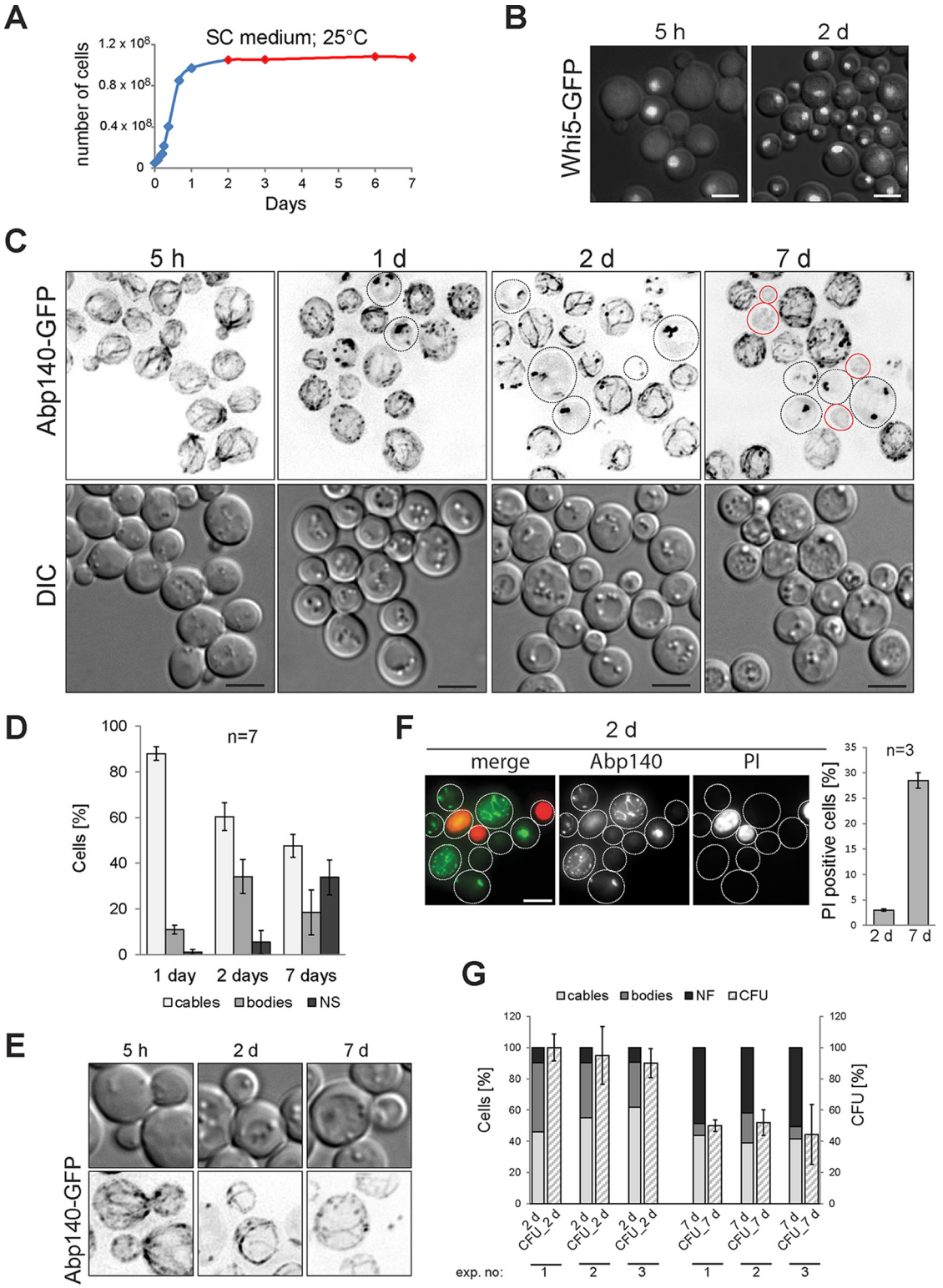

FIG 1 The stationary phase of *S. cerevisiae* is associated with F-actin heterogeneity. The age of the cell cultures is indicated. (A) The growth of a cell culture expressing Abp140-GFP was monitored by cell counting. Blue, exponential and post-diauxic phases; red, stationary phase. (B) A Whi5-GFP fluorescence image (z-stack) merged with a DIC image (opacity, 20%) is shown. (C) Cells expressing Abp140-GFP (WF, z-stack) are shown. Dotted outlines, cells with actin bodies; red outlines, cells with no specific Abp140-GFP fluorescence (NF cells). (D) Stationary-phase cells (expressing Abp140-GFP) with actin structures (cables, bodies, or no fluorescence) were scored. (E) The loss of cable polarity in stationary-phase budded cells expressing Abp140-GFP (WF, z-stack) is shown. (F) Stationary-phase cells expressing Abp140-GFP (z-stack) stained with PI are shown; dotted outlines, the periphery of the cells. PI-positive cells were scored. (G) Cells expressing Abp140-GFP were tested for their clonogenicity. The percentage of CFU and the localization of Abp140-GFP (cables, bodies, or no fluorescence) were plotted for each time point. The results of three independent experiments are shown. d, days. Bars, 4 μm.

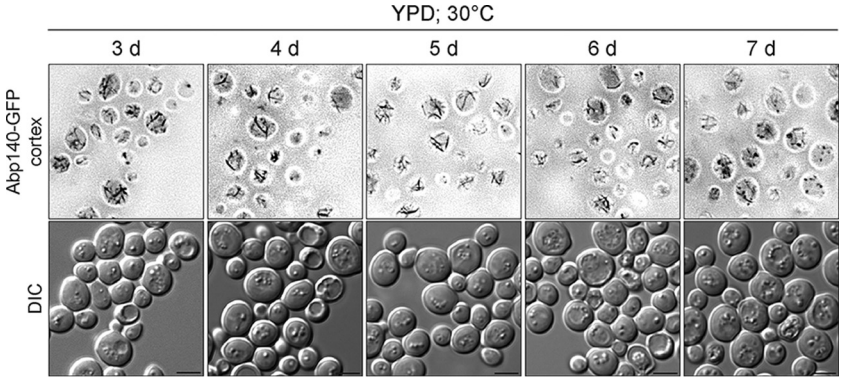

FIG 2 The stationary-phase cells of *S. cerevisiae* grown in rich YPD medium contain actin cables. The cortical layers of cells expressing Abp140-GFP (WF) and DIC images are shown. The age of the cell cultures is indicated. Bars, 4 μm.

tively) and the amount of NF cells was larger (34% ± 8%) in 7-day-old cultures compared with the amounts in 2-day-old cultures. Contrary to the bud-oriented polarity of cables in exponentially growing cells, the cables in all budded stationary-phase cells (2 and 7 days old) lost their orientation along the budded cell axis and became randomly distributed along the cell cortex (Fig. 1E). The loss of the cables' polarity reflected the cessation of cell proliferation and confirmed that the cells had reached the stationary growth phase. To determine the proportion of dead cells, propidium iodide (PI) staining was performed. We found that the 2- and 7-day-old cultures contained 3% and 29% dead cells, respectively. Furthermore, the cells with either cables or actin bodies displayed no PI staining, indicating that they were still alive (Fig. 1F). We also performed a clonogenic assay to determine the amount of cells able to reproduce. We found that cells with cables and cells with actin bodies were able to reproduce, as the percentage of CFU was nearly equal to the sum of the percentages of both groups (Fig. 1G). This result underscores the results of the PI staining experiments and suggests that both groups of cells were alive and had the capacity to reproduce.

Previous observations of the actin cytoskeleton in chronologically aged cells revealed that after glucose exhaustion (the diauxic shift), the cables disappeared and actin bodies were found in the majority of cells within a few hours after the diauxic shift (4). As the cables were visualized in these cells only by phalloidin staining after fixation with formaldehyde, we used the same growth conditions (rich YPD medium, 30°C) described previously (4). We analyzed the distribution of Abp140-GFP in live cells to reveal whether the presence of actin cables in chronologically aged cells depends on the growth conditions or whether the detection of actin structures is influenced by the method of F-actin labeling (*in vivo* with Abp140-GFP or *in vitro* with phalloidin). Interestingly, we found that post-diauxic-phase/stationary-phase cell cultures that were grown in YPD medium were also heterogeneous and also contained cells with cables and NF cells, besides cells with actin bodies (Fig. 2). Note that we present here only the cortical layers of the cells, as chronologically aged cells grown on YPD had strong GFP fluorescence in vacuoles and the presentation of z-stacks decreased the visibility of the cables. In addition, we also labeled the actin cytoskeleton in 2-day-old cultures (SC medium, 25°C) with Alexa-phalloidin after fixation with formaldehyde, and we did not detect, contrary to our *in vivo* observations, any cells with cables (data not shown), confirming the previous observations of fixed cells (4, 10). Altogether, these results indicate that cables are also present in chronologically aged cells grown in rich YPD medium and that phalloidin staining and formaldehyde fixation may destroy actin cables and induce the formation of actin bodies. As the detection of GFP fluorescence and also RFP fluorescence in chronologically aged cells grown in YPD medium is influenced by strong fluorescence in vacuoles, we used SC medium only in further experiments.

Growing cells of *S. cerevisiae* contain two main actin structures, cables and patches. To reveal whether the stationary-phase cells with cables also contain patches, we analyzed a strain expressing Abp140-GFP and the actin bundling protein Sac6-mCherry, commonly used to label patches *in vivo* (43, 44). We found that the cells of the 2-day-old cultures displayed cables, visualized by Abp140-GFP, and patches, decorated by Sac6-mCherry (Fig. 3A). In cells showing the accumulation of Abp140-GFP in actin bodies, Sac6-mCherry lost its cortical localization and accumulated at the same sites as Abp140-GFP. In 7-day-old cultures, we observed a similar phenomenon (not shown). To confirm that branched actin filaments of patches participate in the formation of bodies, we used another marker of patches, actin binding protein Abp1 (45, 46). In 2-day-old cells expressing Sac6-mCherry and Abp1-GFP, we observed that both fluorescent fusions either were localized in patches or accumulated in actin bodies (Fig. 3B). As the actin bodies were recognized by the marker of cables as well as two markers of patches, we suggest that these actin structures are composed of F actin, in which the sites for protein binding cables and patches are maintained.

Altogether, we concluded that F actin is structurally heterogeneous in chronologically aged cells. Two subpopulations of cells

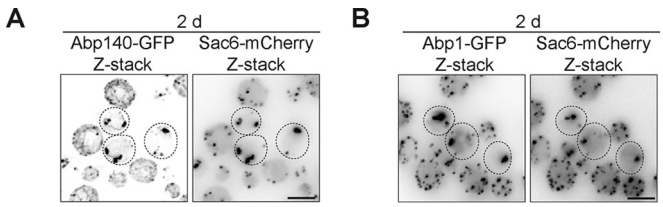

FIG 3 The markers of cortical actin patches also point to F-actin heterogeneity in stationary-phase cells. Two-day-old cells expressing Abp140-GFP (WF; z-stack) and Sac6-mCherry (z-stack) (A) or Abp1-GFP (z-stack) and Sac6-mCherry (z-stack) (B) are shown. Dotted outlines, cells with actin bodies. Bars, 4 μm.

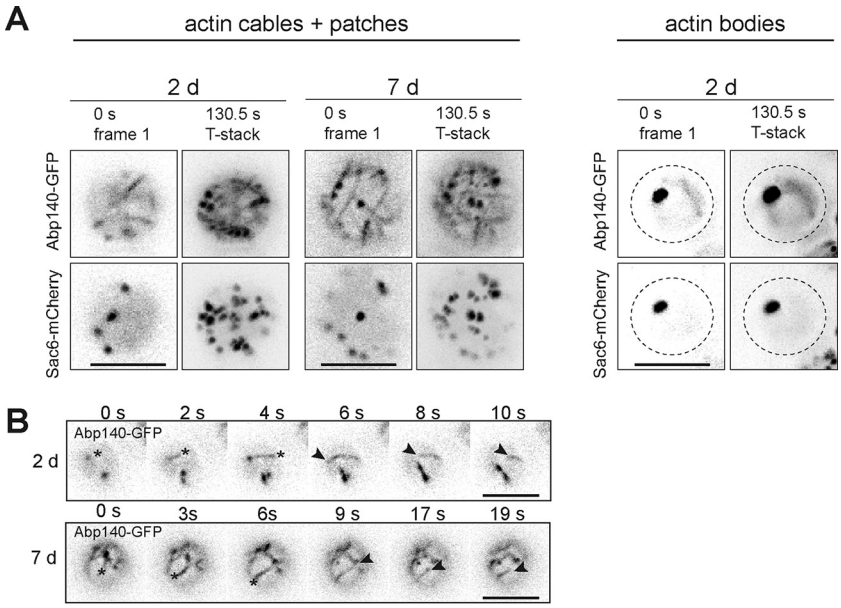

FIG 4 Actin cables and patches in stationary-phase cells preserve cells dynamics. The age of the cell cultures is indicated. (A) Cells expressing Abp140-GFP and Sac6-mCherry were monitored by time-lapse microscopy. The fluorescence in the first frame and T-stack is shown. All images were processed with a no-neighbor (NoNF) filter. (B) Stills of time-lapse images of cells expressing Abp140-GFP (NoNF) are shown; asterisks, the leading end of the cable; arrowheads, the lagging end of the cable. Bars, 4 μm.

with a preserved reproductive capacity could be discriminated, with one displaying both cables (Abp140) and patches (Sac6 and Abp1) and the second one being characterized by actin bodies. The third subpopulation of cells had no specific Abp140-GFP fluorescence, and its ability to reproduce was limited.

Actin cables and patches in chronologically aged cells preserve the dynamics of F actin. To describe the dynamics of F actin in 2- and 7-day-old cultures, we performed time-lapse analyses of cells expressing Abp140-GFP and Sac6-mCherry. Changes in the distribution of both actin markers during the time-lapse recording were evaluated by comparison of the fluorescent signals of the first frame (0 s) and the sum of the signals (maximal projection of frames, T-stack) from all frames (Fig. 4A). Note that in stationary-phase cells with cables (Abp140 signal) and patches (Sac6 signal), the fluorescent signals of both F-actin markers changed their locations with time, indicating a movement of cables and patches even in such aged yeast cells. In the cells containing actin bodies, the localization of Abp140-GFP and Sac6-mCherry remained stable during image acquisition, suggesting that actin bodies are static structures. To perform analysis of the movement of the cables, we used a strain expressing Abp140-GFP and analyzed individual frames obtained by time-lapse microscopy. In stationary-phase cells, we observed cables with an extending leading end together with a moving lagging end (Fig. 4B). These findings indicate that such cables have translational motility, also detected in unpolarized G_1-phase cells (30).

In general, the polymerization and motility of cables depend on formins Bni1 and Bnr1 in cells with polarity and on Bni1 and type V myosin Myo2 in unpolarized cells (30). To elucidate the role of these proteins in chronologically aged cells, we analyzed strains expressing either Bni1-GFP, Bnr1-GFP, or Myo2-GFP. As expected, the localization of all three proteins during the exponential phase of growth was cell cycle dependent. However, their localization typical for cell proliferation was lost in the 2-day-old culture (Fig. 5A). The fluorescence of Bnr1-GFP and Bni1-GFP in these cells was hardly detectable and not distinguishable from autofluorescence. In contrast, in cells expressing Myo2-GFP, we observed dots and cable-like structures in the 2-day-old culture.

As described above, the yeast stationary-phase cells contain either mobile actin cytoskeleton (cables and patches) or static actin bodies. In order to find out whether the localization of Myo2 varies in the context of F-actin structures and whether the translational motility of cables in stationary-phase cells is linked to Myo2, we analyzed a strain expressing Abp140-TagRFP-T and Myo2-GFP. We found that in cells with actin bodies, Myo2-GFP did not localize to these structures, while in cells with cables it formed dots or cable-like structures (Fig. 5B). The analyses of individual layers revealed that Myo2-GFP mainly localized to the cell cortex, where it was next to or overlapping with cables labeled by Abp140-TagRFP-T (Fig. 5C). The examination of individual frames also showed that Myo2-GFP associated with the lagging end as well as the leading end of the cable (Fig. 5D). The localization of Myo2-GFP into the cell cortex and its contact with cables suggest that Myo2 serves as a motor for the sliding of cables along the plasma membrane (translational motility [30]) in 2-day-old cells.

To compare the turnover of G actin in cables, patches, and actin bodies, we treated stationary-phase cells expressing Abp140-GFP and Sac6-mCherry with LatB, which inhibits F-actin polymerization by sequestering G actin (47). We observed that 2- and 7-day-old cultures treated with LatB did not contain cells with cables. Such populations consisted of cells with depolymerized actin (a diffuse cytoplasmic Abp140-GFP or Sac6-mCherry signal), cells with cortical patches, and cells with actin bodies (Fig. 6A). Note that the proportion of cells with patches was higher in 7-day-old cultures than in 2-day-old cultures even after 120

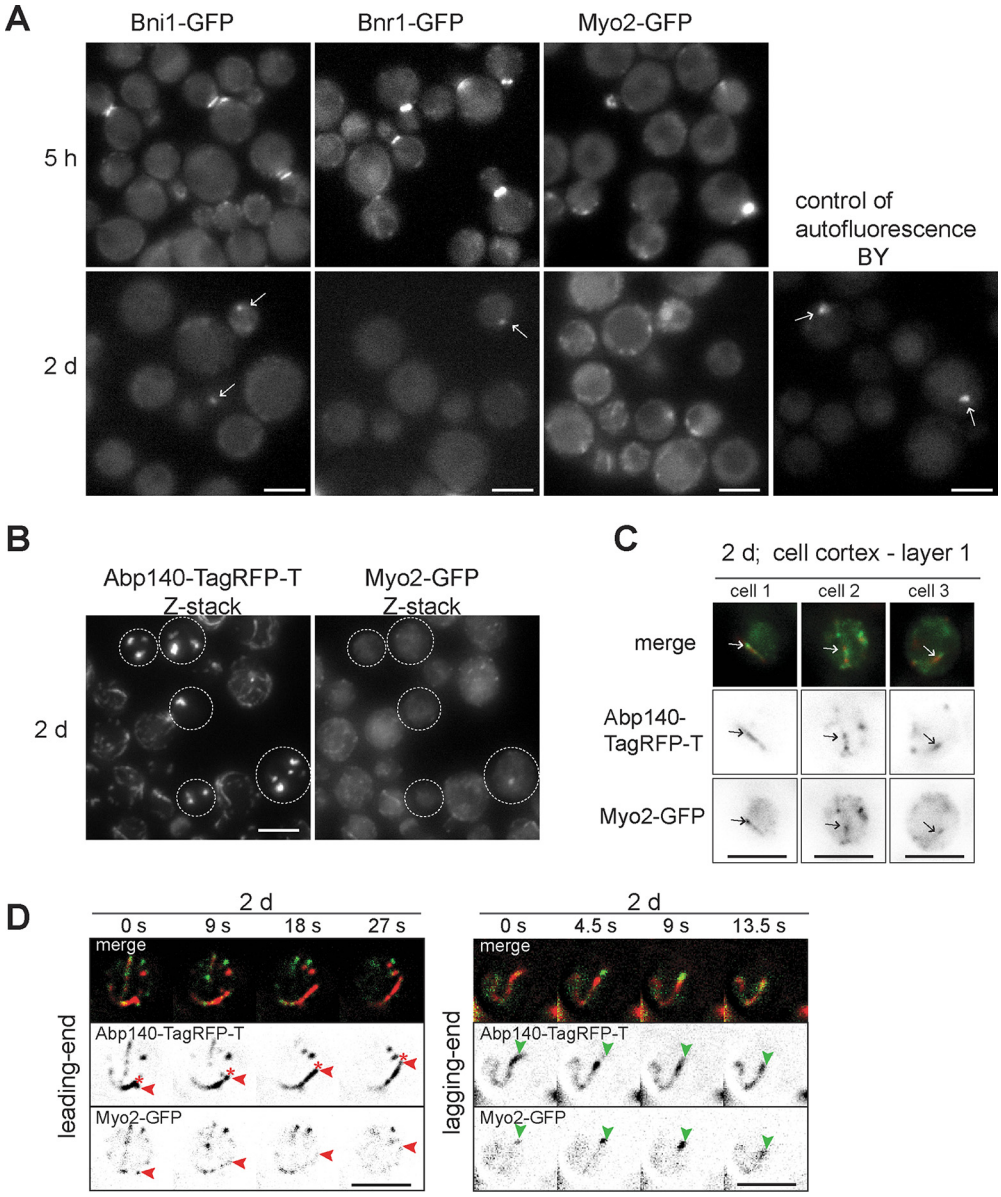

FIG 5 Myo2 associates with actin cables in 2-day-old cells. The age of the cell cultures is indicated. (A) Cells expressing Bni1-GFP, Bnr1-GFP, or Myo2-GFP are shown; the central section is shown. The fluorescence of strain BY without any protein fused to GFP is shown as a control. Arrows, the autofluorescent signal. (B) Cells expressing Abp140-TagRFP-T (z-stack) and Myo2-GFP (z-stack) are shown; dotted outlines, cells with actin bodies. (C) The localization of Myo2-GFP and Abp140-TagRFP-T in the cortex of three individual cells of the same strain shown in panel B is shown. Arrows, the same site of the images. (D) The same strain shown in panel B was analyzed by time-lapse microscopy. Stills of the locations of Abp140-TagRFP-T (NoNF) and Myo2-GFP (NoNF; contrasted) are shown; asterisks, the leading end; red arrowheads, Myo2-GFP on the leading end; green arrowheads, Myo2-GFP on the lagging end. Bars, 4 μm.

min of LatB treatment, pointing to the decreased actin dynamics in older cells (Fig. 6B).

We proved that patches and cables in chronologically aged cells are mobile structures and the F actin in these structures undergoes turnover. In contrast, actin bodies are static structures containing F actin that is not depolymerized. Among the tested proteins responsible for cable dynamics, only Myo2 remained detectable and associated with cables in 2-day-old cells.

The number of cells with actin cables is increased in cultures with a prolonged chronological life span. We found that two live cell populations that can be distinguished by the status of F actin were present in stationary-phase cultures. The next step was to determine which actin structure is associated with the adaptation and survival of cells in the stationary phase. Therefore, we used growth under CR (0.5% glucose), an accepted model known to generate a chronological longevity phenotype (7). The strain expressing Abp140-GFP was grown under CR, and Abp140-GFP localization was observed at several time points of the stationary phase. Unlike cells grown on 2% glucose (Fig. 1C and D), the majority of stationary-phase cells grown under CR contained 94% ± 3%, 87% ± 3%, and 75% ± 9% cables at 2, 7, and 12 days, respectively. Only a few cells displayed actin bodies (Fig. 7A and B), indicating that the actin status correlates with adaptation of the cells to stationary phase. The fitness of populations grown

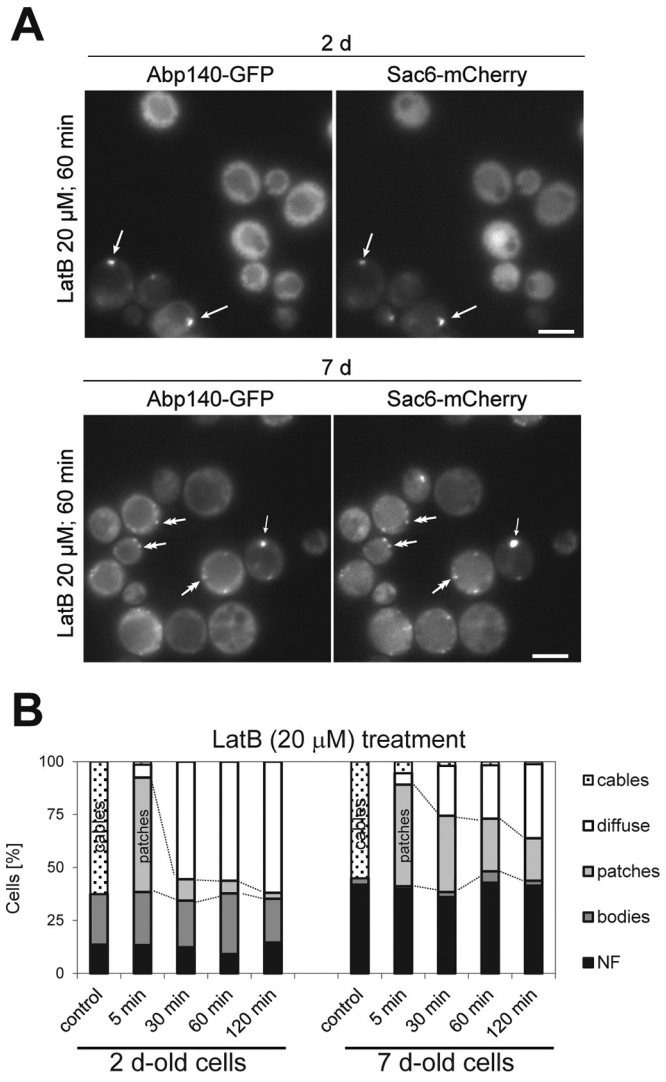

FIG 6 LatB treatment disrupts actin cables in stationary-phase cells. Two- and 7-day-old cells expressing Abp140-GFP and Sac6-mCherry were treated with LatB. The fluorescence of Abp140-GFP and Sac6-mCherry (both central sections) (A) and quantification of Abp140-GFP localization (cables, bodies, patches, diffuse, or no fluorescence) (B) are shown. Single-headed arrows, bodies; double-headed arrows, patches. Bars, 4 μm.

under CR was verified by monitoring of cell viability. Cultures growing under CR for 12 days contained only 3% PI-positive cells, whereas cell populations grown on 2% glucose for the same amount of time contained 75% PI-positive cells (Fig. 7C).

Our findings reveal that an adaptation of *S. cerevisiae* to stationary phase is linked to the persistence of dynamic F-actin structures.

Active endocytosis and autophagy in the stationary-phase cells require a dynamic actin cytoskeleton. As described above, the persisting actin cables seem to be markers of an increased chronological life span. We asked for which processes the actin cytoskeleton might be required during chronological aging. At first, we monitored endocytosis, where actin plays an essential role at the stage of membrane internalization (48). To follow endocytosis in chronologically aged cells, we labeled 2-day-old cultures growing either on 2% glucose or under CR with the lipophilic dye FM4-64. Figure 8A shows that the dye was internalized in the majority of cells containing cables (Abp140-GFP). To confirm that FM4-64 internalization (endocytosis) in 2-day-old cells containing cables depends on F-actin turnover, as was described for growing cells, we treated 2-day-old cells with LatB before addition of FM4-64. As expected, Abp140-GFP was uniformly distributed in the cytoplasm and the internalization of FM4-64 was not detected (Fig. 8B). Finally, this experiment also revealed that the cells with actin bodies displayed no fluorescent signal of the FM4-64 dye.

Another process that might be dependent on a dynamic actin cytoskeleton in stationary-phase cells is autophagy. Although the actin cytoskeleton is dispensable for bulk autophagy, there is evidence that actin is involved in the selective types of autophagy, namely, in cytoplasm-to-vacuole targeting (49, 50) and in the autophagy-dependent delivery of the endoplasmic reticulum into the vacuole (51). To test the links between autophagy and the status of actin in stationary phase, we performed microscopic analyses of 2-day-old cells (grown in either 2% or 0.5% glucose) expressing Abp140-TagRFP-T and GFP-Atg8 derived from the centromeric plasmid. Atg8 regulates the size of the autophagosome, and its vacuolar accumulation indicates the activation of autophagy (52). We found that in the 2-day-old cells, GFP-Atg8 accumulated in the vacuole, and this accumulation corresponded to the presence of cables (Fig. 8C). The cells with actin bodies frequently showed low levels of expression of GFP-Atg8 and low levels of its accumulation in vacuoles. The vacuolar-to-cytoplasmic (V/C) ratios of GFP-Atg8 fluorescence intensity, presented as a scatter dot plot, confirmed a correlation between the presence of cables and the vacuolar accumulation of GFP-Atg8. Cells with cables revealed a higher level of GFP-Atg8 vacuolar accumulation than cells with actin bodies under both culture conditions (2% or 0.5% glucose). Even more, when we compared the V/C ratios of GFP-Atg8 fluorescence in the population of cells with cables grown under CR or on 2% glucose, we found that cells under CR accumulated GFP-Atg8 in the vacuole more efficiently than cells grown on glucose-rich medium.

We also tested the influence of the disruption of F-actin turnover caused by LatB treatment on the GFP-Atg8 distribution. LatB was added to the 1-day-old culture grown under CR, and the culture was incubated for 1 additional day. Destabilization of the cables was confirmed by observation of Abp140-TagRFP-T relocalization either to the cytoplasm or to patches (Fig. 8D). F-actin destabilization led to a heterogeneous response of GFP-Atg8 localization. Although some cells with GFP-Atg8 localized in the vacuole could be still observed, a fraction of the cells with GFP-Atg8 remaining in the cytosol emerged. The V/C ratio revealed that the portion of cells with a lower V/C ratio after LatB treatment significantly increased compared to that in the control population.

Altogether, our experiments reveal that 2-day-old cells containing the dynamic actin cytoskeleton have functional endocytosis and autophagy and the persistence of F-actin turnover is essential for endocytosis and partially also for autophagy.

Actin bodies are not specific markers of replicative age. According to Allen et al., the stationary-phase cell populations contain long-term-lived quiescent (Q) daughter cells and nonquiescent (NQ) mother cells (6). To explore whether the actin status is related to replicative age, we costained stationary-phase cells with the dye calcofluor white M2R (CFW) to visu-

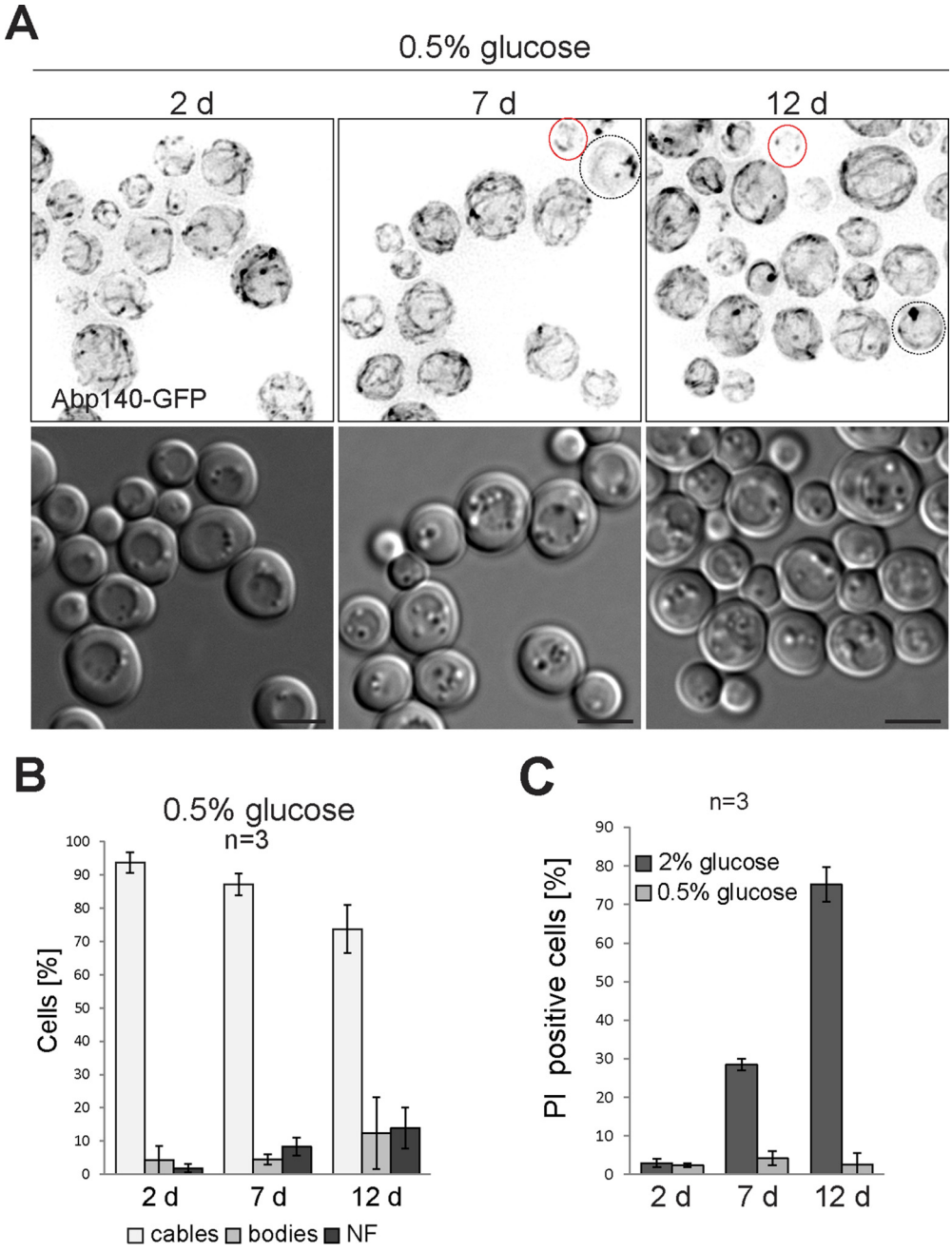

FIG 7 The number of cells with actin cables is increased in cultures with a prolonged chronological life span. The age of the cell culture and the initial concentration of glucose are indicated. (A) Cells expressing Abp140-GFP (z-stack; WF) were grown under CR; dotted outlines, cells with actin bodies; red outlines, NF cells. DIC images are shown. Bars, 4 μm. (B) Stationary-phase cells (from the same experiment for which the results are presented in panel A) were scored for actin structures (cables, bodies, or no fluorescence). (C) Cell cultures used in the experiments whose results are presented in Fig. 1C and panel A were stained with PI. PI-positive cells were scored.

alize bud scars. We found that 2- and 7-day-old cultures consisted mainly of replicatively young cells, as over 80% of daughter cells and young mother cells with 1 or 2 bud scars were present in those cultures (Fig. 9A). We did not identify any cells with 11 or more scars; thus, such replicatively old cells were probably very rare in stationary-phase cultures. We divided the cells into 5 groups according to their replicative age (daughter cells with no scars and mother cells with 1 or 2 scars, 3 or 4 scars, 5 or 6 scars, or 7 to 10 scars) and scored the cells with a particular actin structure in every group. We found that cables, actin bodies, and NF cells were present in all groups, irrespective of their replicative age, in 2-day-old cultures (Fig. 9B). In 7-day-old cultures, we did not identify any cells with cables in the group of cells with 7 to 10 bud scars. Nevertheless, such cells were still present in the group of cells with 5 or 6 bud scars.

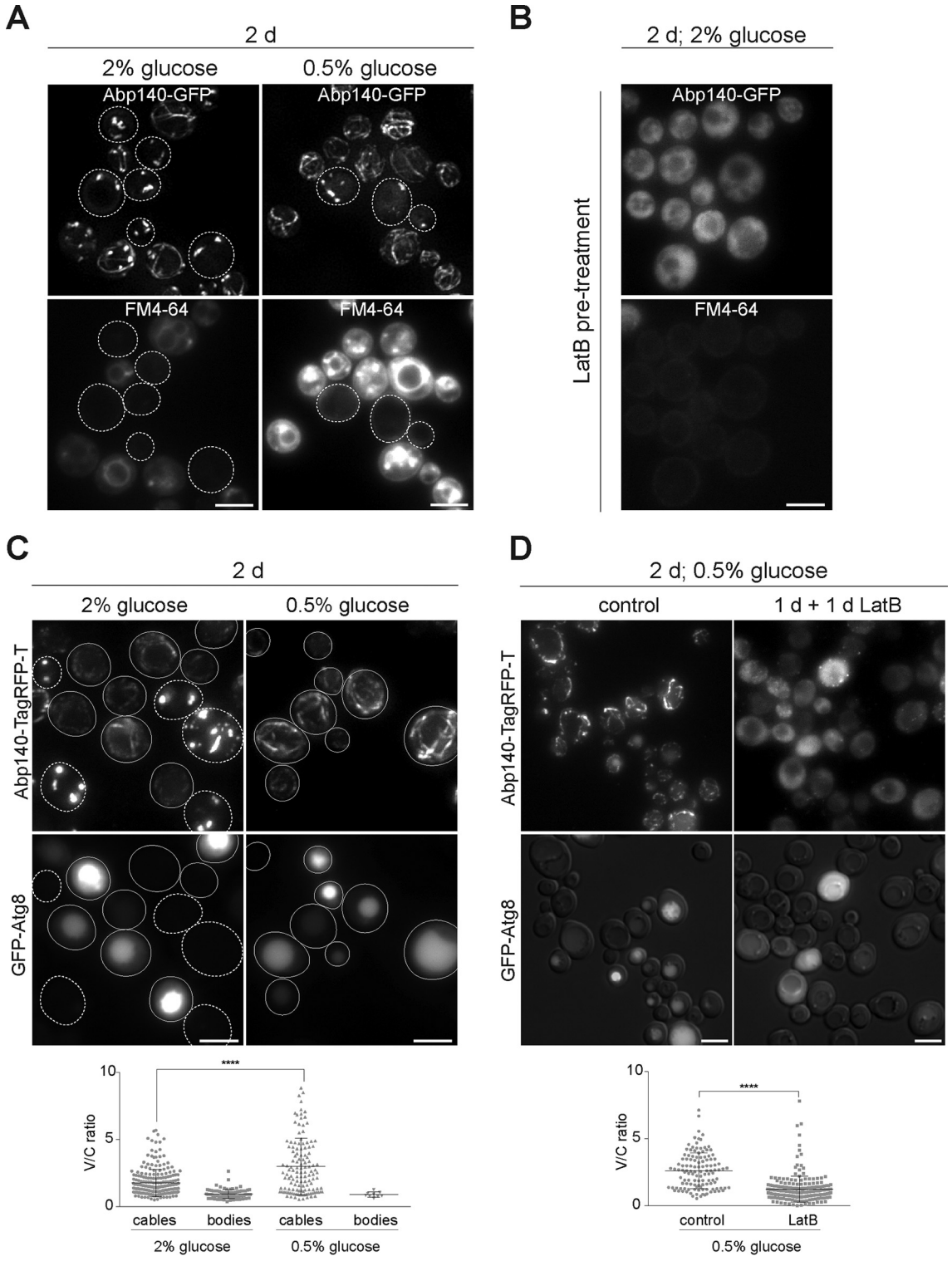

FIG 8 Stationary-phase cells with actin cables reveal active endocytosis and autophagy. The age of the cell cultures and the initial concentration of glucose are indicated. (A) Stationary-phase cells expressing Abp140-GFP were stained with FM4-64. The fluorescence of Abp140-GFP (z-stack) and FM4-64 is shown; dotted outlines, cells with actin bodies. (B) Cells expressing Abp140-GFP (z-stack) were treated with LatB, and then FM4-64 was added. (C) Cells expressing Abp140-TagRFP-T (z-stack) and GFP-Atg8 are shown; solid outlines, cells with actin cables; dotted outlines, cells with actin bodies. (Bottom) Scatter dot plots of V/C ratios are shown. (D) The same strain for which the results are shown in panel C was grown under CR for 1 day, and then LatB or DMSO (the solvent for LatB; control cells) was added and the cells were incubated for 1 additional day. The fluorescence of Abp140-TagRFP-T (z-stack) and merged images of GFP-Atg8 and DIC images (opacity 30%) are shown. (Bottom) Scatter dot plots of V/C ratios are shown. ****, $P < 0.0001$, determined by two-tailed Student's test for the difference between the cells with cables grown in 2% glucose and under CR (graph in panel C) and for the difference between cells treated with LatB and control cells (graph in panel D). Bars, 4 μm.

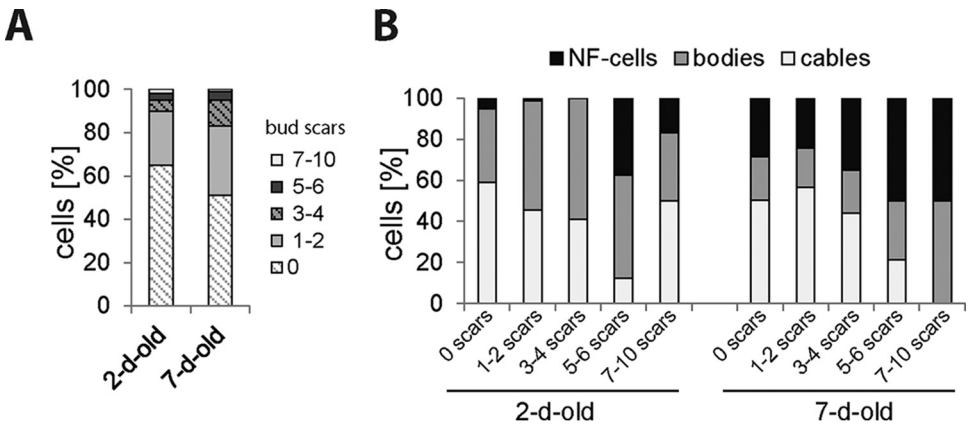

FIG 9 Actin status does not reflect the replicative age of cells. Cells of the 2- and 7-day-old cultures expressing Abp140-GFP were stained with CFW, and then the cells with 0, 1 or 2, 3 or 4, 5 or 6, or 7 to 10 bud scars were counted (A) and the percentages of cells with cables, cells with actin bodies, and NF cells were scored for all subpopulations of different replicative ages (B).

Altogether, the stationary-phase yeast cultures mainly consisted of replicatively young cells. Even these replicatively young cells displayed cables, actin bodies, or no specific Abp140-GFP fluorescence. Thus, the actin cytoskeleton heterogeneity is not directly linked to the replicative age of yeast cells.

Emergence of actin bodies corresponds to respiratory dysfunction in stationary-phase cells. The existence of large actin accumulations has been described in post-diauxic-phase cells defective in actin dynamics (53). These cells also displayed a reduction of the mitochondrial membrane potential and respiratory defects. Since mitochondrial respiration is an essential requirement for stationary-phase adaptation, survival, and life span extension in yeast (54–56), we decided to correlate the actin status with the pattern of mitochondria in chronologically aged cells. We used strains expressing Abp140-TagRFP-T together with either Tom20-GFP (Tom20 is a mitochondrial membrane protein [57]) or Rsm23-GFP (Rsm23 is a mitochondrial ribosomal protein [58]). We analyzed the distribution of Tom20-GFP and Rsm23-GFP, and we found that most of the cells displaying cables contained a developed mitochondrial network (Fig. 10A). In contrast, the cells with actin bodies always contained round mitochondria or a fragmented mitochondrial network, indicating a strong correlation between the status of F actin and the status of the mitochondrial network. Moreover, although 1-day-old post-diauxic-phase cultures contained only 10% of cells with actin bodies, we found that about 40% of the cells of the same culture contained a fragmented mitochondrial network and round mitochondria. This suggests that the structural aberrations of the mitochondria preceded the occurrence of static actin bodies, as shown in Fig. 10B.

In this respect, we wanted to know how these structural aberrations of mitochondria are linked to respiratory dysfunction and how they are linked to the actin status. We used cells containing a dysfunctional cytochrome *c* oxidase (COX) complex. To inactivate the COX complex, we deleted the *COX4* gene in a strain expressing Abp140-TagRFP-T and Tom20-GFP. We analyzed the shape of the mitochondria and actin cytoskeleton of these cells in post-diauxic and stationary phases (1, 2, and 5 days), when the wild-type (WT) yeast metabolism should turn to oxidative metabolism. We found that 1-day-old respiratory activity-deficient *cox4*Δ cells already displayed a fragmented mitochondrial network and round mitochondria (Fig. 11). Abp140-TagRFP-T was localized into the patches in most of the cells, and only a small proportion of cells contained actin bodies or actin cables. However, this was changed in 2-day-old cells, as these cells predominantly contained actin bodies. Some *cox4*Δ cells still revealed a fragmented mitochondrial network labeled with Tom20-GFP, and some cells were without Tom20-GFP fluorescence. The 5-day-old *cox4*Δ culture also contained cells with actin bodies, but the Tom20-GFP fluorescence was not detected in the majority of the cells. Additionally, we analyzed these cells by time-lapse microscopy to follow the actin dynamics (Fig. 11, bottom row). The changes of the actin dynamics are presented as merged images of the Abp140-GFP signal in the first frame (blue) and the sum of the Abp140-GFP signals from all frames (red). The relocalization of Abp140-TagRFP-T in the cell during image capture is visible as a red color. These analyses revealed that 1-day-old respiratory activity-deficient *cox4*Δ cells that already contained a fragmented mitochondrial network and round mitochondria still had a dynamic actin cytoskeleton. The 2- and 5-day-old *cox4*Δ populations predominantly contained cells with static actin bodies.

Altogether, these results confirmed that the fragmentation of the mitochondrial network and the occurrence of round mitochondria might be markers of respiratory dysfunction. Our analyses also indicate that the formation of actin bodies corresponds to mitochondrial dysfunction, which precedes the rearrangement of F actin into static actin bodies.

Actin bodies are markers of reduced cell fitness rather than dying cells. Notably, populations of the post-diauxic-phase respiratory-deficient *cox4*Δ mutant did not contain cells with cables. We utilized this state of the culture lacking cells with cables to test the link between the ability to reproduce and the status of the actin cytoskeleton. First, we compared the clonogenicity of *cox4*Δ cells with that of WT cells cultured for 1, 2, and 3 days. We found that nearly all *cox4*Δ cells as well as WT cells of the 1-day-old culture were able to grow on plates containing glucose (proportion of CFU, 100%). However, during aging, the *cox4*Δ cells lost this ability more rapidly than WT cells (in 2-day-old cultures, the proportion of WT cell CFU was 100% and that of *cox4*Δ cell CFU was 74%; in 3-day-old cultures, the proportion of WT cell CFU was 86% and that of *cox4*Δ cell CFU was 48%) (Fig. 12A). Interestingly, the obtained percentage of CFU corresponded to the per-

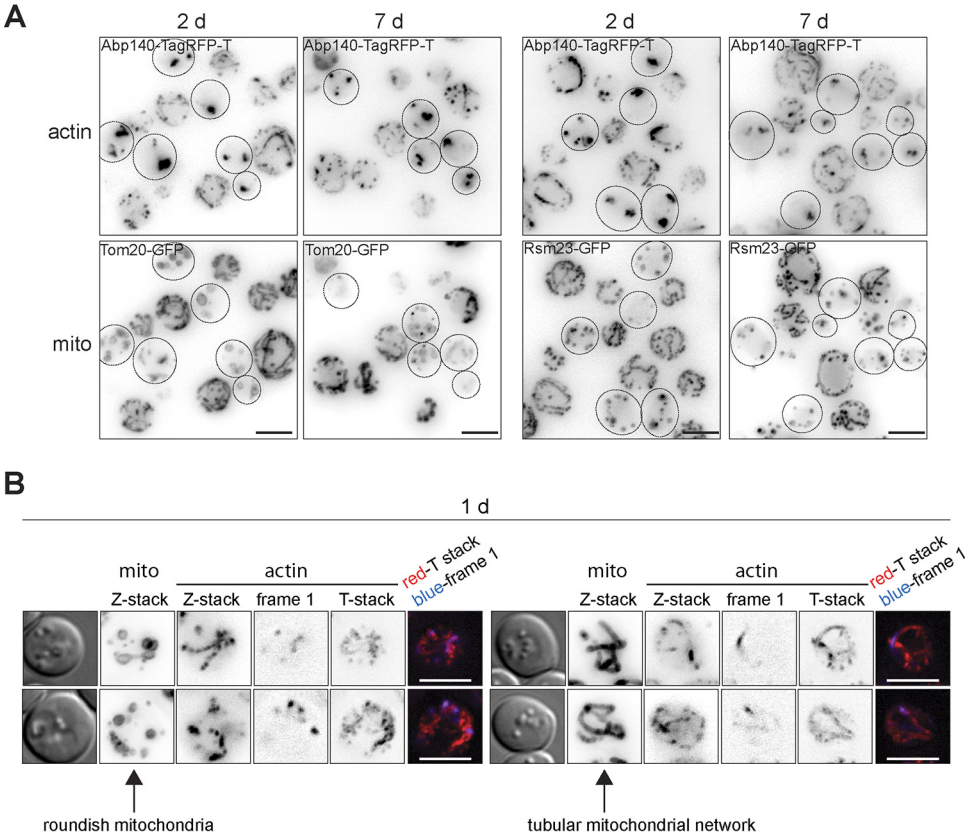

FIG 10 Cells containing actin bodies reveal an aberrant shape of mitochondria (mito). The age of the cell cultures is indicated. (A) Cells expressing Abp140-TagRFP-T and Tom20-GFP or Rsm23-GFP are shown. Images are presented as z-stacks; dashed outlines, cell with actin bodies. (B) Cells expressing Abp140-tagRFP-T and Tom20-GFP are shown. Images of the same cells were captured first by time-lapse microscopy and then by Z-sectioning. The images show, from the left, DIC image, Tom20-GFP (z-stack), Abp140-tagRFP-T (z-stack), Abp140-tagRFP-T (first frame; NoNF), Abp140-tagRFP-T (T-stack; NoNF), and merge of the first frame and T-stack. The left set of images shows examples of cells with an aberrant mitochondrial network; the right set shows examples of cells with a tubular mitochondrial network. Bars, 4 μm.

centage of cells with actin bodies (in 1-day-old cultures, the sum of cells with patches and cells with actin bodies) in each individual experiment (Fig. 12B). Consistent with the finding that the majority of cells containing actin bodies were still able to reproduce, actin bodies were able to recover into a dynamic actin cytoskeleton within 5 min after glucose addition (Fig. 12C).

These results indicate that the formation of actin bodies visualized by Abp140 fluorescent fusions is not a marker of dying yeast cells.

DISCUSSION

Live-imaging studies helped provide an understanding of the behavior of the *S. cerevisiae* actin cytoskeleton (30, 59), but this approach has mainly been utilized in exponentially growing cultures. Investigations of fixed cells have revealed that actin bodies are the only F-actin structure of post-diauxic-phase/stationary-phase cells (4, 10). Herein we present *in vivo* observations of the actin cytoskeleton in stationary-phase cells that extend the common knowledge. We present evidence that the stationary-phase cultures consist not only of cells with actin bodies but also of cells with a dynamic actin cytoskeleton (cables and patches). Our findings point to the heterogeneity of the cells in the stationary-phase cultures and to the important function of actin in cell adaptation to the stationary phase.

It has previously been shown on fixed cells that cables disappear at the diauxic shift when the glucose is exhausted. Then, within a few hours actin bodies have been found in the majority of post-diauxic-phase cells (4). Contrary to these findings, our experimental approach employing only *in vivo* observations of various actin cytoskeleton markers revealed the persistence of cells with cables, besides the cells with actin bodies, even in 7-day-old cultures. We observed this heterogeneity of the actin status in live stationary-phase cells that were grown in different media. For the majority of our experiments, we used the synthetic SC medium that is recommended for use in chronological aging studies (60), and in addition, it is suitable for use for observation of live cells by fluorescence microscopy. Further, we analyzed the persistence of actin cables in cells that were grown under CR in SC medium, conditions that extend the chronological life span. Since Sagot et al. (4) analyzed the actin cytoskeleton in the cells that were grown in YPD, we also analyzed the actin cytoskeleton in cells growing in this rich medium, though this medium is less suitable for use in live-imaging studies because of autofluorescence. Thus, using a different medium, we confirmed that the persistence of actin cables is not a unique metabolic program activated only in stationary-phase cells that are grown in SC medium. We conclude that the

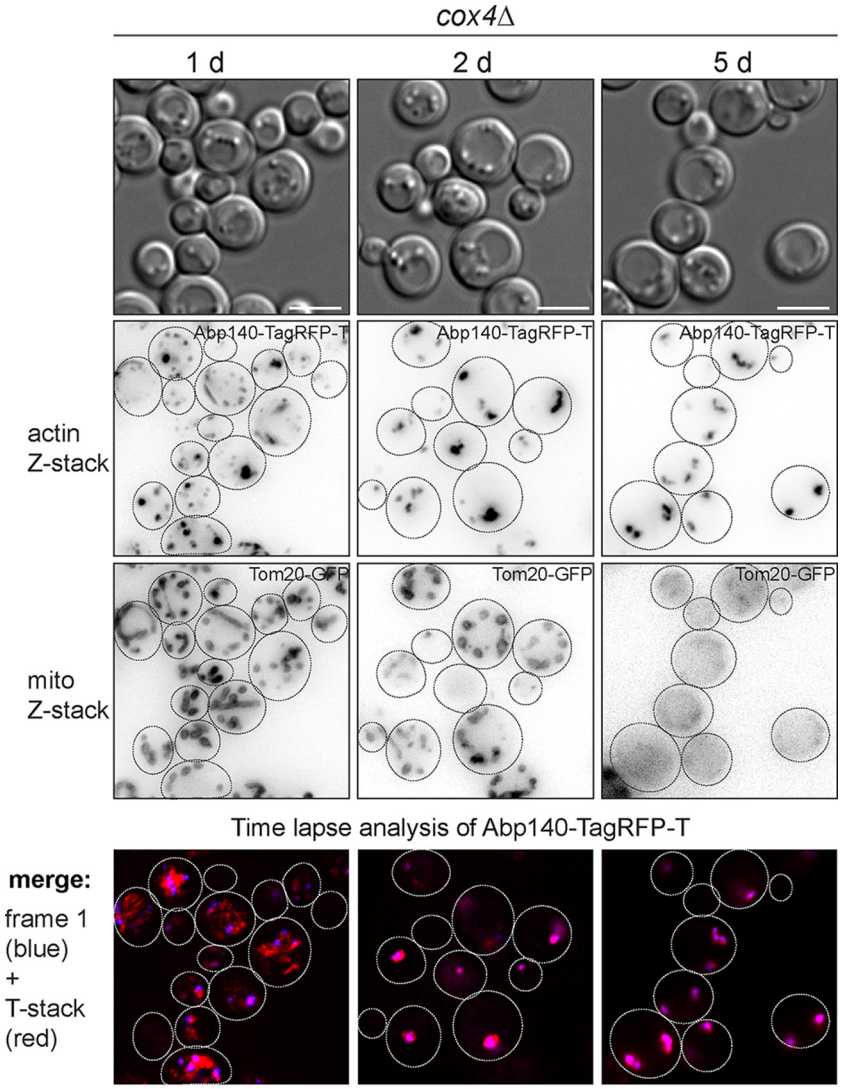

FIG 11 The occurrence of mitochondrial network aberrations precedes the formation of static actin bodies. The age of the cell cultures is indicated. *cox4*Δ cells expressing Abp140-TagRFP-T and Tom20-GFP are shown. Images of the same cells were captured first by time-lapse microscopy and then by z-sectioning. DIC images, images of cells expressing Abp140-TagRFP-T (z-stack), images of cells expressing Tom20-GFP (z-stack), and the dynamics of Abp140-TagRFP-T (merge of first frame and T-stack of cortical layers; NoNF) are presented from the top to the bottom, respectively; dashed outlines, the periphery of the cells. Bars, 4 μm.

occurrence of cells with cables and cells with bodies seems to be associated with each chronologically aged population.

Why are there differences between the observations of Sagot et al. (4) and our observations? Unlike us, those authors used phalloidin staining after formaldehyde fixation. Therefore, we applied the same *in vitro* labeling of F actin in 2-day-old cultures (SC medium, 25°C), and we also did not find any cells containing cables but detected only cells with actin bodies. Similarly, recent observations of the actin cytoskeleton in live glucose-depleted cells revealed the presence of cables (31) that were not previously detected in fixed cells (32). Thus, our results are supported by these observations, and we conclude that *in vivo* studies may extend the knowledge obtained on fixed cells.

Despite all the differences in experimental approaches, the actin bodies that we observed *in vivo* had characteristics similar to those of the actin bodies described by Sagot et al. (4). These authors showed that (i) Abp140-GFP, Abp1-GFP, and Sac6-GFP colocalize with F actin in actin bodies, (ii) actin bodies are stable structures resistant to LatB treatment, and (iii) actin bodies are able to disappear after addition of glucose.

Our data show that cells in stationary phase can be divided into two live subpopulations on the basis of their actin status. Similarly, other authors also claim that the stationary-phase culture is divided into two subpopulations, dense Q daughter cells and NQ cells (5, 6, 10). These authors suggested that only daughter cells and in some circumstances young mother cells can acquire characteristics of quiescence. Q daughter cells are unbudded, long-term-surviving cells with the ability to reproduce. They arrest in the G_1 phase of the cell cycle, contain well-developed mitochondria, and use respiration to produce ATP. Here we described a subpopulation of cells with cables and patches exhibiting some characteristics similar to those of Q daughter cells. Both Q daugh-

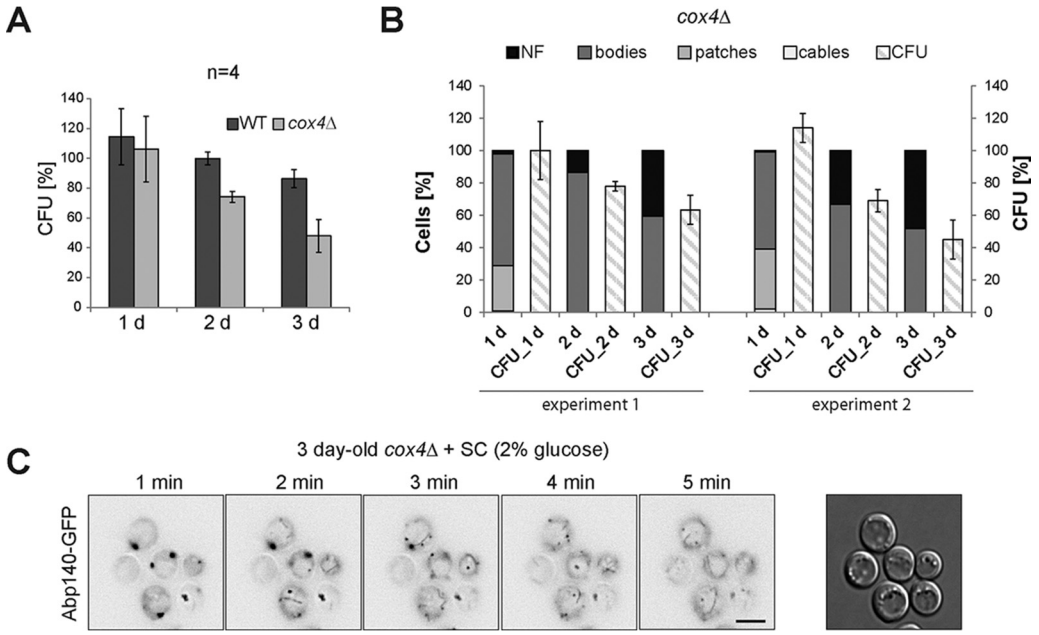

FIG 12 Actin bodies are markers of reduced cell fitness but not of dying cells. The age of the cell cultures is indicated. (A) WT and *cox4*Δ cells expressing Abp140-GFP were analyzed by the clonogenic assay. The percentages of CFU obtained were plotted. (B) The results of two independent experiments analyzing the relation between the percentages of CFU and the localization of Abp140-GFP (cables, patches, bodies, or no fluorescence) in stationary-phase cells (*cox4*Δ cells expressing Abp140-GFP) are shown. (C) SC medium was added to a 3-day-old cell culture (*cox4*Δ cells expressing Abp140-GFP), and the recovery of actin was monitored by time-lapse microscopy. Still images of Abp140-GFP (NoNF) at the indicated time points are shown. Image capture started 1 min after SC medium was added. Bar, 4 μm.

ter cells and cells with dynamic actin are well adapted for survival, as they contain developed mitochondrial networks. However, by determining the replicative age, we found that these groups are not identical, as the subpopulation of cells with dynamic actin consisted not only of daughter cells but also of mother cells. This situation resembles a new model for the differentiation of Q and NQ cells (61). This recent model shows that cell fate is decided at or before glucose exhaustion. Then, in post-diauxic phase, NQ mother cells produce NQ daughter cells and Q mother cells produce Q daughter cells. Importantly, according to these authors, the main characteristic of Q cells (mother and daughter cells) is their metabolic/respiratory activity, albeit these cells appear to be quiescent.

The cessation of cell division is not the only response to nutrient scarcity during the transition into the stationary phase. The stationary-phase cells also actively respond to these changes and must remain metabolically and biosynthetically active, albeit at reduced levels (3). Our results support this concept, as we found that the presence of the dynamic actin accompanied by persisting endocytosis, autophagy, and respiration points to better adaptation to the stationary phase.

The impact of autophagy on better survival in the stationary phase has already been described (8, 9, 62). As in some other studies (9, 63, 64), we confirmed the activation of autophagy in the early stationary phase (2-day-old cultures). We used GFP-Atg8, which is a marker of both types of macroautophagy, selective and nonselective macroautophagy (14). The observed decline in the level of GFP-Atg8 vacuolar accumulation after actin cytoskeleton disruption using LatB treatment of stationary-phase cells indicates that some types of selective macroautophagy may contribute to this process in stationary-phase cells.

Endocytosis was another process active in stationary-phase cells with dynamic actin. We observed FM4-64 internalization in the 2-day-old yeast culture, and we proved that it depends on F actin. In respect to endocytosis, its activation in yeast stationary-phase cells has not been described yet. The only data pointing to the activation of endocytosis upon starvation have recently been published (65). The authors described the presence of active endocytosis upon acute glucose depletion and proposed that the endocytic internalization of proteins and lipids from the plasma membrane contributes to cell catabolism. Genome-wide screens also identified several endosomal proteins for which deletion of their genes caused shortening of the chronological life span (8). Even more, the possibility that autophagy-unrelated degradation processes contribute to yeast chronological survival was taken into consideration (66).

Our results indicate that autophagy and endocytosis are mainly active in the early stationary phase, as in 7-day-old cultures the amount of cells containing GFP-Atg8 in the vacuole dropped significantly and the efficiency of FM4-64 internalization was also lower than that in 2-day-old cultures (data not shown). These observations point to the fact that stationary-phase cells gradually change their metabolism. This indicates that endocytosis and also autophagy are active only when the substrates degraded through these routes are still present. This concept of the gradual utilization of various substrates is supported by our observations that in 7-day-old cells with cables the mitochondrial markers were localized not only to mitochondria but also to the vacuole, which indicates the activation of mitophagy (see Movie S1 in the supplemental material).

Our experiments revealed that the occurrence of actin bodies in stationary-phase cells correlates with morphological

changes to the mitochondrial network (a fragmented mitochondrial network and round mitochondria). Similar morphological changes of mitochondria were observed in post-diauxic-phase cells of a respiratory activity-deficient (*cox4*Δ) strain. Additionally, our experiments indicate that such morphological changes of mitochondrial networks preceded the rearrangement of F actin into static actin bodies. In this respect, a direct relationship between the appearance of actin aggregates and mitochondrial dysfunction has been observed previously (29, 53, 67, 68). It has been shown that genetic interventions causing decreased actin dynamics resulted in the formation of large actin aggregates in the early stationary phase and that cells with the aggregates were unable to activate mitochondria (29, 53). Therefore, in contrast to our results, these authors supposed that the formation of actin aggregates leads to the dysfunction of mitochondria. Despite these contradictions, we concur that the emergence of actin aggregates/bodies in post-diauxic-phase and stationary-phase cells points to decreased fitness.

The survival of yeast stationary-phase cells mainly relies on the stores of nutrients (glycogen and trehalose) and their efficient utilization performed by mitochondrial respiration (10, 11). The dysfunction of mitochondria in cells in the post-diauxic phase results in the utilization of storage components by glycolysis, which is less efficient in gaining energy than respiration (10). Thus, the formation of static actin bodies may indicate the status of critical levels of energy. This phenomenon resembles the situation in neurites of neurons, where the transient formation of rod-like actin inclusions (ADF/cofilin rods) has also been observed (69). These structures were formed when the synthesis of ATP was inhibited, and their formation transiently protected neurites from the unnecessary consumption of ATP (70). Similarly, the formation of yeast actin bodies may also minimize the consumption of ATP and thus facilitate the longer survival of respiration-deficient cells.

ACKNOWLEDGMENTS

We are grateful to Zdenek Hodny for discussions and critical reading of the manuscript. The assistance provided by D. Janoskova and D. Haskova is acknowledged.

This work was supported by CSF P305/12/0480.

REFERENCES

1. **Kaeberlein M.** 2010. Lessons on longevity from budding yeast. Nature **464:**513–519. http://dx.doi.org/10.1038/nature08981.
2. **Longo VD, Finch CE.** 2003. Evolutionary medicine: from dwarf model systems to healthy centenarians? Science **299:**1342–1346. http://dx.doi.org/10.1126/science.1077991.
3. **Gray JV, Petsko GA, Johnston GC, Ringe D, Singer RA, Werner-Washburne M.** 2004. "Sleeping beauty": quiescence in Saccharomyces cerevisiae. Microbiol Mol Biol Rev **68:**187–206. http://dx.doi.org/10.1128/MMBR.68.2.187-206.2004.
4. **Sagot I, Pinson B, Salin B, Daignan-Fornier B.** 2006. Actin bodies in yeast quiescent cells: an immediately available actin reserve? Mol Biol Cell **17:**4645–4655. http://dx.doi.org/10.1091/mbc.E06-04-0282.
5. **Shi L, Sutter BM, Ye X, Tu BP.** 2010. Trehalose is a key determinant of the quiescent metabolic state that fuels cell cycle progression upon return to growth. Mol Biol Cell **21:**1982–1990. http://dx.doi.org/10.1091/mbc.E10-01-0056.
6. **Allen C, Buttner S, Aragon AD, Thomas JA, Meirelles O, Jaetao JE, Benn D, Ruby SW, Veenhuis M, Madeo F, Werner-Washburne M.** 2006. Isolation of quiescent and nonquiescent cells from yeast stationary-phase cultures. J Cell Biol **174:**89–100. http://dx.doi.org/10.1083/jcb.200604072.
7. **Smith DL, Jr, McClure JM, Matecic M, Smith JS.** 2007. Calorie restriction extends the chronological lifespan of Saccharomyces cerevisiae independently of the sirtuins. Aging Cell **6:**649–662. http://dx.doi.org/10.1111/j.1474-9726.2007.00326.x.
8. **Fabrizio P, Hoon S, Shamalnasab M, Galbani A, Wei M, Giaever G, Nislow C, Longo VD.** 2010. Genome-wide screen in Saccharomyces cerevisiae identifies vacuolar protein sorting, autophagy, biosynthetic, and tRNA methylation genes involved in life span regulation. PLoS Genet **6:**e1001024. http://dx.doi.org/10.1371/journal.pgen.1001024.
9. **Alvers AL, Fishwick LK, Wood MS, Hu D, Chung HS, Dunn WA, Jr, Aris JP.** 2009. Autophagy and amino acid homeostasis are required for chronological longevity in Saccharomyces cerevisiae. Aging Cell **8:**353–369. http://dx.doi.org/10.1111/j.1474-9726.2009.00469.x.
10. **Li L, Miles S, Melville Z, Prasad A, Bradley G, Breeden LL.** 2013. Key events during the transition from rapid growth to quiescence in budding yeast require posttranscriptional regulators. Mol Biol Cell **24:**3697–3709. http://dx.doi.org/10.1091/mbc.E13-05-0241.
11. **Ocampo A, Liu J, Schroeder EA, Shadel GS, Barrientos A.** 2012. Mitochondrial respiratory thresholds regulate yeast chronological life span and its extension by caloric restriction. Cell Metab **16:**55–67. http://dx.doi.org/10.1016/j.cmet.2012.05.013.
12. **Bonawitz ND, Rodeheffer MS, Shadel GS.** 2006. Defective mitochondrial gene expression results in reactive oxygen species-mediated inhibition of respiration and reduction of yeast life span. Mol Cell Biol **26:**4818–4829. http://dx.doi.org/10.1128/MCB.02360-05.
13. **Toshima JY, Toshima J, Kaksonen M, Martin AC, King DS, Drubin DG.** 2006. Spatial dynamics of receptor-mediated endocytic trafficking in budding yeast revealed by using fluorescent alpha-factor derivatives. Proc Natl Acad Sci U S A **103:**5793–5798. http://dx.doi.org/10.1073/pnas.0601042103.
14. **Monastyrska I, Rieter E, Klionsky DJ, Reggiori F.** 2009. Multiple roles of the cytoskeleton in autophagy. Biol Rev Camb Philos Soc **84:**431–448. http://dx.doi.org/10.1111/j.1469-185X.2009.00082.x.
15. **Higuchi R, Vevea JD, Swayne TC, Chojnowski R, Hill V, Boldogh IR, Pon LA.** 2013. Actin dynamics affect mitochondrial quality control and aging in budding yeast. Curr Biol **23:**2417–2422. http://dx.doi.org/10.1016/j.cub.2013.10.022.
16. **Adams AE, Pringle JR.** 1984. Relationship of actin and tubulin distribution to bud growth in wild-type and morphogenetic-mutant Saccharomyces cerevisiae. J Cell Biol **98:**934–945. http://dx.doi.org/10.1083/jcb.98.3.934.
17. **Young ME, Cooper JA, Bridgman PC.** 2004. Yeast actin patches are networks of branched actin filaments. J Cell Biol **166:**629–635. http://dx.doi.org/10.1083/jcb.200404159.
18. **Huckaba TM, Gay AC, Pantalena LF, Yang HC, Pon LA.** 2004. Live cell imaging of the assembly, disassembly, and actin cable-dependent movement of endosomes and actin patches in the budding yeast, Saccharomyces cerevisiae. J Cell Biol **167:**519–530. http://dx.doi.org/10.1083/jcb.200404173.
19. **Idrissi FZ, Blasco A, Espinal A, Geli MI.** 2012. Ultrastructural dynamics of proteins involved in endocytic budding. Proc Natl Acad Sci U S A **109:**E2587–E2594. http://dx.doi.org/10.1073/pnas.1202789109.
20. **Moseley JB, Goode BL.** 2006. The yeast actin cytoskeleton: from cellular function to biochemical mechanism. Microbiol Mol Biol Rev **70:**605–645. http://dx.doi.org/10.1128/MMBR.00013-06.
21. **Sagot I, Klee SK, Pellman D.** 2002. Yeast formins regulate cell polarity by controlling the assembly of actin cables. Nat Cell Biol **4:**42–50.
22. **Pruyne D, Gao L, Bi E, Bretscher A.** 2004. Stable and dynamic axes of polarity use distinct formin isoforms in budding yeast. Mol Biol Cell **15:**4971–4989. http://dx.doi.org/10.1091/mbc.E04-04-0296.
23. **Smethurst DG, Dawes IW, Gourlay CW.** 2014. Actin—a biosensor that determines cell fate in yeasts. FEMS Yeast Res **14:**89–95. http://dx.doi.org/10.1111/1567-1364.12119.
24. **Delley PA, Hall MN.** 1999. Cell wall stress depolarizes cell growth via hyperactivation of RHO1. J Cell Biol **147:**163–174. http://dx.doi.org/10.1083/jcb.147.1.163.
25. **Desrivieres S, Cooke FT, Parker PJ, Hall MN.** 1998. MSS4, a phosphatidylinositol-4-phosphate 5-kinase required for organization of the actin cytoskeleton in Saccharomyces cerevisiae. J Biol Chem **273:**15787–15793. http://dx.doi.org/10.1074/jbc.273.25.15787.
26. **Chowdhury S, Smith KW, Gustin MC.** 1992. Osmotic stress and the yeast cytoskeleton: phenotype-specific suppression of an actin mutation. J Cell Biol **118:**561–571. http://dx.doi.org/10.1083/jcb.118.3.561.

27. **Yuzyuk T, Foehr M, Amberg DC.** 2002. The MEK kinase Ssk2p promotes actin cytoskeleton recovery after osmotic stress. Mol Biol Cell **13:**2869–2880. http://dx.doi.org/10.1091/mbc.02-01-0004.
28. **Farah ME, Sirotkin V, Haarer B, Kakhniashvili D, Amberg DC.** 2011. Diverse protective roles of the actin cytoskeleton during oxidative stress. Cytoskeleton **68:**340–354. http://dx.doi.org/10.1002/cm.20516.
29. **Gourlay CW, Ayscough KR.** 2005. Identification of an upstream regulatory pathway controlling actin-mediated apoptosis in yeast. J Cell Sci **118:**2119–2132. http://dx.doi.org/10.1242/jcs.02337.
30. **Yu JH, Crevenna AH, Bettenbuhl M, Freisinger T, Wedlich-Soldner R.** 2011. Cortical actin dynamics driven by formins and myosin V. J Cell Sci **124:**1533–1541. http://dx.doi.org/10.1242/jcs.079038.
31. **Xu L, Bretscher A.** 2014. Rapid glucose depletion immobilizes active myosin V on stabilized actin cables. Curr Biol **24:**2471–2479. http://dx.doi.org/10.1016/j.cub.2014.09.017.
32. **Uesono Y, Ashe MP, Toh EA.** 2004. Simultaneous yet independent regulation of actin cytoskeletal organization and translation initiation by glucose in Saccharomyces cerevisiae. Mol Biol Cell **15:**1544–1556. http://dx.doi.org/10.1091/mbc.E03-12-0877.
33. **Huh WK, Falvo JV, Gerke LC, Carroll AS, Howson RW, Weissman JS, O'Shea EK.** 2003. Global analysis of protein localization in budding yeast. Nature **425:**686–691. http://dx.doi.org/10.1038/nature02026.
34. **Baudin A, Ozier-Kalogeropoulos O, Denouel A, Lacroute F, Cullin C.** 1993. A simple and efficient method for direct gene deletion in Saccharomyces cerevisiae. Nucleic Acids Res **21:**3329–3330. http://dx.doi.org/10.1093/nar/21.14.3329.
35. **Chalfie M, Tu Y, Euskirchen G, Ward WW, Prasher DC.** 1994. Green fluorescent protein as a marker for gene expression. Science **263:**802–805. http://dx.doi.org/10.1126/science.8303295.
36. **Gueldener U, Heinisch J, Koehler GJ, Voss D, Hegemann JH.** 2002. A second set of loxP marker cassettes for Cre-mediated multiple gene knockouts in budding yeast. Nucleic Acids Res **30:**e23. http://dx.doi.org/10.1093/nar/30.6.e23.
37. **Sheff MA, Thorn KS.** 2004. Optimized cassettes for fluorescent protein tagging in Saccharomyces cerevisiae. Yeast **21:**661–670. http://dx.doi.org/10.1002/yea.1130.
38. **Shaner NC, Lin MZ, McKeown MR, Steinbach PA, Hazelwood KL, Davidson MW, Tsien RY.** 2008. Improving the photostability of bright monomeric orange and red fluorescent proteins. Nat Methods **5:**545–551. http://dx.doi.org/10.1038/nmeth.1209.
39. **Gietz RD, Schiestl RH.** 2007. High-efficiency yeast transformation using the LiAc/SS carrier DNA/PEG method. Nat Protoc **2:**31–34. http://dx.doi.org/10.1038/nprot.2007.13.
40. **Yang HC, Pon LA.** 2002. Actin cable dynamics in budding yeast. Proc Natl Acad Sci U S A **99:**751–756. http://dx.doi.org/10.1073/pnas.022462899.
41. **Costanzo M, Nishikawa JL, Tang X, Millman JS, Schub O, Breitkreuz K, Dewar D, Rupes I, Andrews B, Tyers M.** 2004. CDK activity antagonizes Whi5, an inhibitor of G_1/S transcription in yeast. Cell **117:**899–913. http://dx.doi.org/10.1016/j.cell.2004.05.024.
42. **Bean JM, Siggia ED, Cross FR.** 2006. Coherence and timing of cell cycle start examined at single-cell resolution. Mol Cell **21:**3–14. http://dx.doi.org/10.1016/j.molcel.2005.10.035.
43. **Doyle T, Botstein D.** 1996. Movement of yeast cortical actin cytoskeleton visualized in vivo. Proc Natl Acad Sci U S A **93:**3886–3891. http://dx.doi.org/10.1073/pnas.93.9.3886.
44. **Smith MG, Swamy SR, Pon LA.** 2001. The life cycle of actin patches in mating yeast. J Cell Sci **114:**1505–1513.
45. **Goode BL, Rodal AA, Barnes G, Drubin DG.** 2001. Activation of the Arp2/3 complex by the actin filament binding protein Abp1p. J Cell Biol **153:**627–634. http://dx.doi.org/10.1083/jcb.153.3.627.
46. **Drubin DG, Miller KG, Botstein D.** 1988. Yeast actin-binding proteins: evidence for a role in morphogenesis. J Cell Biol **107:**2551–2561. http://dx.doi.org/10.1083/jcb.107.6.2551.
47. **Ayscough KR, Stryker J, Pokala N, Sanders M, Crews P, Drubin DG.** 1997. High rates of actin filament turnover in budding yeast and roles for actin in establishment and maintenance of cell polarity revealed using the actin inhibitor latrunculin-A. J Cell Biol **137:**399–416. http://dx.doi.org/10.1083/jcb.137.2.399.
48. **Galletta BJ, Mooren OL, Cooper JA.** 2010. Actin dynamics and endocytosis in yeast and mammals. Curr Opin Biotechnol **21:**604–610. http://dx.doi.org/10.1016/j.copbio.2010.06.006.
49. **He C, Song H, Yorimitsu T, Monastyrska I, Yen WL, Legakis JE, Klionsky DJ.** 2006. Recruitment of Atg9 to the preautophagosomal structure by Atg11 is essential for selective autophagy in budding yeast. J Cell Biol **175:**925–935. http://dx.doi.org/10.1083/jcb.200606084.
50. **Monastyrska I, He C, Geng J, Hoppe AD, Li Z, Klionsky DJ.** 2008. Arp2 links autophagic machinery with the actin cytoskeleton. Mol Biol Cell **19:**1962–1975. http://dx.doi.org/10.1091/mbc.E07-09-0892.
51. **Hamasaki M, Noda T, Baba M, Ohsumi Y.** 2005. Starvation triggers the delivery of the endoplasmic reticulum to the vacuole via autophagy in yeast. Traffic **6:**56–65. http://dx.doi.org/10.1111/j.1600-0854.2004.00245.x.
52. **Suzuki K, Kirisako T, Kamada Y, Mizushima N, Noda T, Ohsumi Y.** 2001. The pre-autophagosomal structure organized by concerted functions of APG genes is essential for autophagosome formation. EMBO J **20:**5971–5981. http://dx.doi.org/10.1093/emboj/20.21.5971.
53. **Gourlay CW, Carpp LN, Timpson P, Winder SJ, Ayscough KR.** 2004. A role for the actin cytoskeleton in cell death and aging in yeast. J Cell Biol **164:**803–809. http://dx.doi.org/10.1083/jcb.200310148.
54. **Bonawitz ND, Chatenay-Lapointe M, Pan Y, Shadel GS.** 2007. Reduced TOR signaling extends chronological life span via increased respiration and upregulation of mitochondrial gene expression. Cell Metab **5:**265–277. http://dx.doi.org/10.1016/j.cmet.2007.02.009.
55. **Aerts AM, Zabrocki P, Govaert G, Mathys J, Carmona-Gutierrez D, Madeo F, Winderickx J, Cammue BP, Thevissen K.** 2009. Mitochondrial dysfunction leads to reduced chronological lifespan and increased apoptosis in yeast. FEBS Lett **583:**113–117. http://dx.doi.org/10.1016/j.febslet.2008.11.028.
56. **Pan Y, Schroeder EA, Ocampo A, Barrientos A, Shadel GS.** 2011. Regulation of yeast chronological life span by TORC1 via adaptive mitochondrial ROS signaling. Cell Metab **13:**668–678. http://dx.doi.org/10.1016/j.cmet.2011.03.018.
57. **Sollner T, Griffiths G, Pfaller R, Pfanner N, Neupert W.** 1989. MOM19, an import receptor for mitochondrial precursor proteins. Cell **59:**1061–1070. http://dx.doi.org/10.1016/0092-8674(89)90762-9.
58. **Saveanu C, Fromont-Racine M, Harington A, Ricard F, Namane A, Jacquier A.** 2001. Identification of 12 new yeast mitochondrial ribosomal proteins including 6 that have no prokaryotic homologues. J Biol Chem **276:**15861–15867. http://dx.doi.org/10.1074/jbc.M010864200.
59. **Kaksonen M, Sun Y, Drubin DG.** 2003. A pathway for association of receptors, adaptors, and actin during endocytic internalization. Cell **115:**475–487. http://dx.doi.org/10.1016/S0092-8674(03)00883-3.
60. **Longo VD, Fabrizio P.** 2012. Chronological aging in Saccharomyces cerevisiae. Subcell Biochem **57:**101–121. http://dx.doi.org/10.1007/978-94-007-2561-4_5.
61. **Davidson GS, Joe RM, Roy S, Meirelles O, Allen CP, Wilson MR, Tapia PH, Manzanilla EE, Dodson AE, Chakraborty S, Carter M, Young S, Edwards B, Sklar L, Werner-Washburne M.** 2011. The proteomics of quiescent and nonquiescent cell differentiation in yeast stationary-phase cultures. Mol Biol Cell **22:**988–998. http://dx.doi.org/10.1091/mbc.E10-06-0499.
62. **Matecic M, Smith DL, Pan X, Maqani N, Bekiranov S, Boeke JD, Smith JS.** 2010. A microarray-based genetic screen for yeast chronological aging factors. PLoS Genet **6:**e1000921. http://dx.doi.org/10.1371/journal.pgen.1000921.
63. **Aris JP, Alvers AL, Ferraiuolo RA, Fishwick LK, Hanvivatpong A, Hu D, Kirlew C, Leonard MT, Losin KJ, Marraffini M, Seo AY, Swanberg V, Westcott JL, Wood MS, Leeuwenburgh C, Dunn WA, Jr.** 2013. Autophagy and leucine promote chronological longevity and respiration proficiency during calorie restriction in yeast. Exp Gerontol **48:**1107–1119. http://dx.doi.org/10.1016/j.exger.2013.01.006.
64. **Ruckenstuhl C, Netzberger C, Entfellner I, Carmona-Gutierrez D, Kickenweiz T, Stekovic S, Gleixner C, Schmid C, Klug L, Sorgo AG, Eisenberg T, Buttner S, Marino G, Koziel R, Jansen-Durr P, Frohlich KU, Kroemer G, Madeo F.** 2014. Lifespan extension by methionine restriction requires autophagy-dependent vacuolar acidification. PLoS Genet **10:**e1004347. http://dx.doi.org/10.1371/journal.pgen.1004347.
65. **Lang MJ, Martinez-Marquez JY, Prosser DC, Ganser LR, Buelto D, Wendland B, Duncan MC.** 2014. Glucose starvation inhibits autophagy via vacuolar hydrolysis and induces plasma membrane internalization by down-regulating recycling. J Biol Chem **289:**16736–16747. http://dx.doi.org/10.1074/jbc.M113.525782.
66. **Longo VD, Nislow C, Fabrizio P.** 2010. Endosomal protein sorting and autophagy genes contribute to the regulation of yeast life span. Autophagy **6:**1227–1228. http://dx.doi.org/10.4161/auto.6.8.13850.
67. **Gourlay CW, Ayscough KR.** 2006. Actin-induced hyperactivation of the

Ras signaling pathway leads to apoptosis in Saccharomyces cerevisiae. Mol Cell Biol **26:**6487–6501. http://dx.doi.org/10.1128/MCB.00117-06.

68. **Leadsham JE, Miller K, Ayscough KR, Colombo S, Martegani E, Sudbery P, Gourlay CW.** 2009. Whi2p links nutritional sensing to actin-dependent Ras-cAMP-PKA regulation and apoptosis in yeast. J Cell Sci **122:**706–715. http://dx.doi.org/10.1242/jcs.042424.
69. **Minamide LS, Striegl AM, Boyle JA, Meberg PJ, Bamburg JR.** 2000. Neurodegenerative stimuli induce persistent ADF/cofilin-actin rods that disrupt distal neurite function. Nat Cell Biol **2:**628–636. http://dx.doi.org/10.1038/35023579.
70. **Bernstein BW, Chen H, Boyle JA, Bamburg JR.** 2006. Formation of actin-ADF/cofilin rods transiently retards decline of mitochondrial potential and ATP in stressed neurons. Am J Physiol Cell Physiol **291:**C828–C839. http://dx.doi.org/10.1152/ajpcell.00066.2006.